https://doi.org/10.5194/egusphere-2025-4375
Preprint. Discussion started: 17 September 2025

Global geomagnetic response to repetitive geospace storm of March 21–25, 2024

Leonid F. Chernogor[1]

[1]Space Radio Physics, V. N. Karazin Kharkiv National University, Kharkiv, 61022, Ukraine

Correspondence to: Leonid F. Chernogor (Leonid.F.Chernogor@gmail.com)

Abstract. The geomagnetic storm of March 21–26, 2024, was comprised of five storms, i.e., it was a multi-step storm, with the main storm occurring during March 24–25, 2024. A multi-step nature of this storm is unique to this event, and this storm is due to isolated sheaths that appeared in the solar wind. The power of the geospace storms caused by increases in the solar wind dynamic pressure was close to 29 TW, 33 TW, 50 TW, 174 TW, and 192 TW, and their energy did not exceed 0.73 EJ, 0.59 EJ, 0.36 EJ, 2.5 EJ, and 2.8 EJ. The power of the magnetospheric storms being due to increases in the interplanetary magnetic pressure were 13 GJ/s, 13 GJ/s, 130 GJ/s, 1000 GJ/s, and 190 GJ/s, and their energy attained 90 TJ, 90 TJ, 1360 TJ, 22,000 TJ, and 2000 TJ. The energetics of the magnetic and kinetic pressures has been shown to be close to each other. The maximum power of the geomagnetic storms was close to 93 GW, 97 GW, 208 GW, 283 GW, and 89 GW, and their energy were smaller than 3 PJ, 1.4 PJ, 3 PJ, 5.1 PJ, and 4.5 PJ. The storms of March 21–22, 2024; March 23, 2024; March 23–24, 2024; March 24–25, 2024; and March 25–26, 2024, pertain to the storm classes G1 (minor), G1 (minor), G2 (moderate), G4 (severe), and G0 (very minor). In both the eastern and western hemispheres, the peak-to-peak amplitude of variations in a geomagnetic field strength exhibited a tendency to increase with increasing magnetic latitude. At high latitude stations, the peak-to-peak amplitude attained a maximum value of ~1000–2000 nT, whereas at mid- and low latitude stations they were observed to be within ~100–300 nT. The observed possible deviations from the tendency indicated above may be due to the different physical processes acting to cause variations in the geomagnetic field at high, middle, and low latitudes. The peak-to-peak amplitude of variations in a geomagnetic field strength was observed to be the greatest during sunlit hours. The peak-to-peak amplitude of variations in a geomagnetic field strength during the storms was a factor of up to 23–28, 19–23, and 15–19 greater than that during quiet time reference period, in the northward *X*-, eastward *Y*-, and vertical *Z*-component of the geomagnetic field, respectively. The storm of March 24–25, 2024, termed the main storm, was the most intense of all five storms of March 21–26, 2024. The main storm of March 24–25, 2024, is comparable to the storm of April of 23–24, 2023, with respect to all its parameters. At the same time, it is less intense than the storm of May 10–11, 2024, the strongest storm of solar cycle 25, and even less intense than the Carrington event.

https://doi.org/10.5194/egusphere-2025-4375
Preprint. Discussion started: 17 September 2025

1 Introduction

The powerful nonstationary processes on the Sun termed the solar storms are associated with solar flares, producing solar energetic particles, coronal mass ejections (CMEs), high-speed solar wind streams, and shock waves. As a result, the pan-planetary storm appears at the earth that includes the magnetospheric storm, ionospheric storm, atmospheric storm, lithospheric storm, and the storms in all geophysical fields — magnetic, electric, baric, and thermal ones. The geomagnetic storm is the most important constituent, which is dealt in an enormous volume of literature; here mention is made only of a few reviews (Gonzalez et al., 1994, Laštovička, 1997; Danilov, 2013; Mendillo, 2006).

If solar cycle 24 (2009–2019) was relatively quiet, then solar cycle 25 cannot be said to be such a period. A list of only the most intense geomagnetic storms includes the storms of November 3–5, 2021 ($K_{p\max}$ = 8$_-$) (Kim et al., 2023a, 2023b; Regi et al., 2022, Zhai et al., 2023; Chernogor and Tkachenko, 2024); of April 23–24, 2023 ($K_{p\max}$ = 8$_+$) (Hu et al., 2025; Zalizovski et al., 2023); of November 4–7, 2023 ($K_{p\max}$ = 7$_+$) (Agyei-Yeboah, et al., 2025; Ponomarchuk and Zolotukhina, 2024); of March 24, 2024 ($K_{p\max}$ = 8) (Wu et al., 2025; Mavromichalaki et al., 2024; Terefe et al., 2025); of May 10–11, 2024 ($K_{p\max}$ = 9) (Grandin et al., 2024; Pierrard et al., 2025, Yamazaki et al., 2024; Hajra et al., 2024b); of August 12–13, 2024 ($K_{p\max}$ = 8) (Yadav et al., 2025); of September 12, 2024 ($K_{p\max}$ = 7) (Yadav et al., 2025); of September 17, 2024 ($K_{p\max}$ = 8) (Yadav et al., 2025); of October 8, 2024 ($K_{p\max}$ = 7) (Pierrard et al., 2025); of October 10, 2024 ($K_{p\max}$ = 9$_-$) (Pierrard et al., 2025; Correira et al., 2025; Yadav et al., 2025); of January 1, 2025 ($K_{p\max}$ = 8); of April 15–16, 2025 ($K_{p\max}$ = 8$_-$); and of June 1–3, 2025 ($K_{p\max}$ = 8$_-$).

The storm of April 23–24, 2023, pertains to one of the most intense storms of the current solar cycle, with the prominent feature being its two-step nature due to the shock sheath and the magnetic cloud in the CME arriving sequentially (Chernogor, 2025a; Ghag et al., 2024). The energetics of this storm has been analyzed in detail in (Chernogor, 2025b). The effects of the ionospheric storm of April 23–24, 2023, are described in (Souza et al., 2024; Tilahun et al., 2023). The effects of the geomagnetic storm of April 23–24, 2023, are studied in papers (Chernogor, 2025a; Adushkin et al., 2023; Despirak et al., 2024). The processes accompanying the geospace storm of April 23–24, 2023, are revealed by Chernogor (2025a), Hajra et al. (2024a), and Ghag et al. (2024). The effects of the atmospheric storm of April 23–24, 2023, are dealt with in (Souza et al., 2024). The features of the electrical storm of April 23–24, 2023, are analyzed in papers by Adushkin et al. (2023), Souza et al. (2024), and the effects in the baric field are described in the work by Adushkin et al. (2023). The works listed above show that the pan-planetary storm of April 23–24, 2023, manifests itself in all geophysical shells and geophysical fields. The storm is associated with intense aurorae even at middle latitudes (Chernogor, 2025b).

The strongest in solar cycle 25 pan-planetary storm of May 10–11, 2024, termed the Mother's Day storm, is studied even in more detail. The processes operating on the Sun and in geospace are analyzed in papers by Hayakawa (2024) and Kruparova (2024). The energetics of the physical processes associated with the pan-planetary storm of May 8–12, 2024, have been analyzed in detail in the work by Chernogor (2025c). The effects observed during the geomagnetic storm of May 10–11, 2024, are described by Chernogor et al. (2025b) and Yan and Yao (2024), who analyze the global response of the

https://doi.org/10.5194/egusphere-2025-4375
Preprint. Discussion started: 17 September 2025

geomagnetic field to the storm and determine the basic characteristics of latitudinal and diurnal variations in geomagnetic field strengths.

Numerous studies investigate the *ionospheric storm* in May 2024, employing multi-instrument observations of the state of the ionosphere (Spogli et al., 2024; Karan et al., 2024; Evans et al., 2024; Guo et al., 2024; Huang, 2025; Bojilova, 2024; Aa et al., 2024; Singh et al., 2024; Ram et al., 2024; Xia et al., 2024; Themens et al., 2024; Sun et al., 2024; Vichare and Bagiya, 2024; Chernogor and Bessarabova, 2025). The longitudinal and latitudinal dependences of disturbances in the electron density and total electron content have been studied. Specific features in the formation of the equatorial ionization anomaly and polar tongue of ionization are detected. The main phase of the geomagnetic storm corresponds to the negative ionospheric storm, and the recovery phase does to the positive ionospheric storm.

Certain manifestations of the *atmospheric storm* of May 10–11, 2024, are described in the works by Parker et al. (2024), Evans et al. (2024), Xia et al. (2024), Ranjan at al. (2024); the storm is accompanied by additional satellite drag. The results of calculations of the *electrical storm* parameters are presented in (Yan and Yao, 2024). The storm effects in the *thermal field* are discussed in (Evans et al., 2024; Ranjan et al., 2024; Mlynczak et al., 2024). The power of infrared emission is estimated to exceed ~1 TW. Thus, the storm of May 8–12, 2024, pertains to extreme pan-planetary storms that are accompanied by significant disturbances in all geospheres and geophysical fields.

The main feature of the March 21–25, 2024, storm is its repeatability, for the storm consisted of five consecutive geomagnetic storms pertaining to the storm classes from G0 to G4. The most intensive storm, storm class G4 (severe), occurred on March 24, 2024.

The present study investigates a global response in the geomagnetic field to the repeating storms of March 2024.

In this paper we first briefly describe the raw data, and then analyze the state of space weather. Further, the temporal variations in the northward *X*-, eastward *Y*-, and vertical *Z*-component of the geomagnetic field, which have been observed at the magnetometer stations located in both the eastern and western hemispheres, are dealt with. Next, the energetics of all five storms is estimated, the most intense storm of March 24, 2024, is compared with that of other storms of both solar cycle 25 and super unique Carrington-like event. Then, the obtained results are discussed, which is followed by a list of main results. Plots of temporal variations in the three components of the geomagnetic field strength acquired by the magnetometer stations in the eastern and western hemispheres during March 21–27, 2024, are included in the Appendix A and B, respectively.

2 Data and Method

The raw data have been acquired at the magnetometer recording stations included in the International Real-time Magnetic Observatory Network (INTERMAGNET) (https://www.intermagnet.org/). Those stations that are located along a certain meridian in each hemisphere and are chosen for this study are shown in Fig. 1 and listed in Tables 1 and 2. It is well known that the data are available with 1-min time resolution and 1-nT strength resolution (INTERMAGNET Technical Reference Manual, Version 5.0.0, St-Louis, B., Ed.). The daily means for each day are first calculated for each station, which are

https://doi.org/10.5194/egusphere-2025-4375
Preprint. Discussion started: 17 September 2025

subsequently subtracted from the originally observed *X*-, *Y*-, and *Z*-components of the geomagnetic field. As a result, the peak-to-peak amplitudes of variations subjected to further analysis are obtained.

To reveal the effects of the geomagnetic storm, the peak-to-peak amplitudes of variations in the strength of the geomagnetic field on the days when the storms occurred (March 21, 23, 24 and 25, 2024) and on quiet time reference days (March 22 and 27, 2024) are compared.

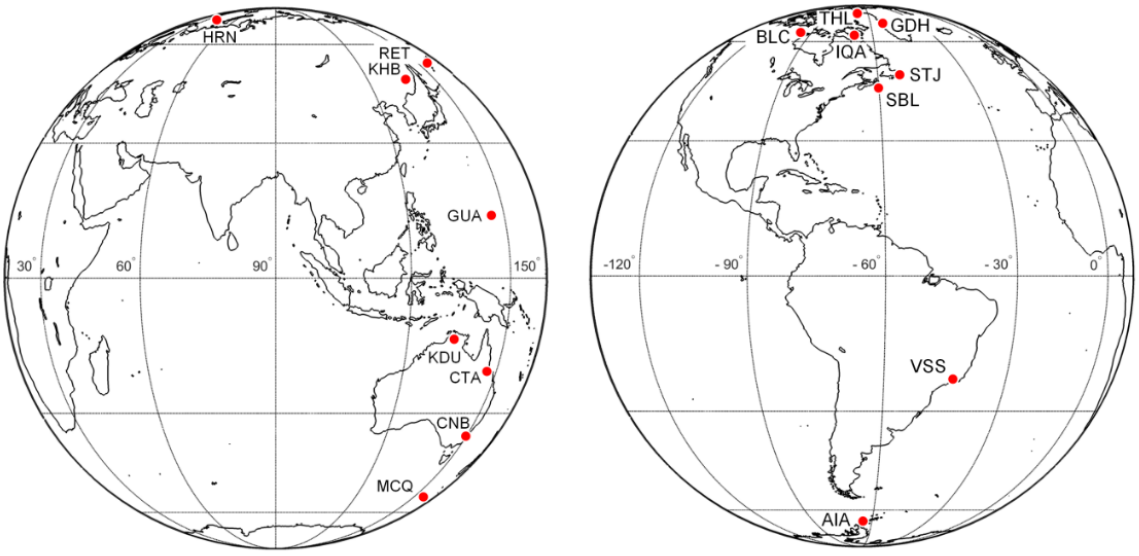

Figure 1. Map of magnetometer stations.

Table 1. Eastern hemisphere stations, sunrise and sunset times.

	Observatory (Name, IAGA Code, Country)	Geographic lat./long.	Geomagnetic lat./long.	Sunrise/Sunset at 0 km altitude	Sunrise/Sunset at 200 km altitude
1	Hornsund, HRN, Norway	77.0000°N, 15.5500°E	+74.28°, +123.35°	04:02/ 18:02	PD*
2	Paratunka (Petropavlovsk), PET, Russia	52.9710°N, 158.2480°E	+46.47° –137.04°	19:13/ 07:52	17:31/ 09:34
3	Khabarovsk, KHB, Russia	47.6100°N, 134.6900°E	+39.09°, –156.40°	20:50/ 09:21	19:20/ 10:51
4	Guam, GUA, United States of America	13.5900°N, 144.8700°E	+6.14°, –143.44°	20:19/ 08:30	19:19/ 09:30
5	Kakadu, KDU, Australia	12.6900°S, 132.4700°E	–20.91°, –153.67°	21:14/ 09:15	20:15/ 10:15
6	Charters Towers, CTA, Australia	20.0900°S, 146.2640°E	–27.01° –138.50°	20:21/ 08:20	19:19/ 09:21
7	Canberra, CNB, Australia	35.3200°S, 149.3600°E	–41.72°, –132.85°	20:11/ 08:04	19:00/ 09:15
8	Macquarie Island, MCQ, Australia	54.5000°S, 158.9500°E	–59.29°, –116.47°	19:37/ 07:18	17:55/ 09:00

* PD stands for polar day

https://doi.org/10.5194/egusphere-2025-4375
Preprint. Discussion started: 17 September 2025

Table 2. Western hemisphere stations, sunrise and sunset times.

	Observatory (Name, IAGA Code, Country)	Geographic lat./long.	Geomagnetic lat./long.	Sunrise/Sunset at 0 km altitude	Sunrise/Sunset at 200 km altitude
1	Qaanaaq (Thule), THL, Greenland	77.4700°N, 69.2270°W	+86.54°, +12.48°	09:39/ 23:47	PD*
2	Qeqertarsuaq (Godhavn), GDH, Greenland	69.2520°N, 53.5330°W	+77.48°, +32.56°	09:04/ 22:18	05:38/ 01:44
3	Iqaluit, IQA, Canada	63.7530°N, 68.5180°W	+72.78°, +6.21°	10:12/ 23:10	07:43/ 01:39
4	Baker Lake, BLC, Canada	64.3180°N, 96.0120°W	+72.27°, –34.57°	12:00/ 00:59	09:29/ 03:30
5	St John's, STJ, Canada	47.5950°N, 52.6770°W	+55.95°, +24.38°	09:22/ 21:55	07:52/ 23:24
6	Sable Island, SBL, Canada	43.9321°N, 60.0095°W	+52.69°, +15.12°	09:51/ 22:21	08:27/ 23:44
7	Vassouras, VSS, Brazil	22.4000°S, 43.6500°W	–14.15°, +27.56°	09:03/ 21:01	08:00/ 22:04
8	Akademik Vernadsky, AIA, Antarctica	65.2450°S, 64.2580°W	–55.96°, +6.30°	10:38/ 22:09	08:13/ 00:33

* PD stands for polar day

3 Space Weather State

The analysis of the state of space weather is based on the OMNI data obtained from the GSFC/SPDF OMNIWeb interface at https://omniweb.gsfc.nasa.gov (https://omniweb.gsfc.nasa.gov/form/dx1.html) (King and Papitashvili, 2004). In this section, the time variations in the solar wind parameters and geomagnetic indices are analyzed (Fig. 2). To enable a better understanding of the mechanisms governing an actual storm, the energetics of the solar wind and a disturbance of the Earth's magnetic field are additionally calculated.

Significant increases in the solar wind proton density n_{sw} occur on March 21, 23, 24, and 25, 2024, and on March 23, 2024, two enhancements are evident. The most notable increase occurs near UT noon on March 23, 2024, when it attains a maximum value of about 4.8×10^7 m^{-3}. In total, five enhancements in n_{sw} are registered from March 21, 2024, to March 25, 2024.

The radial plasma flow speed V_{sw} exhibits fluctuations from an undisturbed value of ~300 km s^{-1} until the middle of the day on March 23, 2024, and it gradually increases from ~300 km s^{-1} to ~450 km s^{-1} over the next 24 h. Approximately at noon on March 24, 2024, it shows a sharp increase from ~450 km s^{-1} to ~800 km s^{-1} followed by fluctuations within ~800–850 km s^{-1} over the next ~9 h, further it reduces from ~800 km s^{-1} to ~700 km s^{-1} over the next ~9 h. The next increase, 6 h in duration, up to ~800 km s^{-1} occurs during the day on March 25, 2024. The latter is followed by a reduction in V_{sw} from ~800 km s^{-1} to ~550 km s^{-1} over 20 h. The last insignificant increase, 12 h in duration, in V_{sw} up to ~650 km s^{-1} is observed to occur on March 26, 2024.

https://doi.org/10.5194/egusphere-2025-4375
Preprint. Discussion started: 17 September 2025

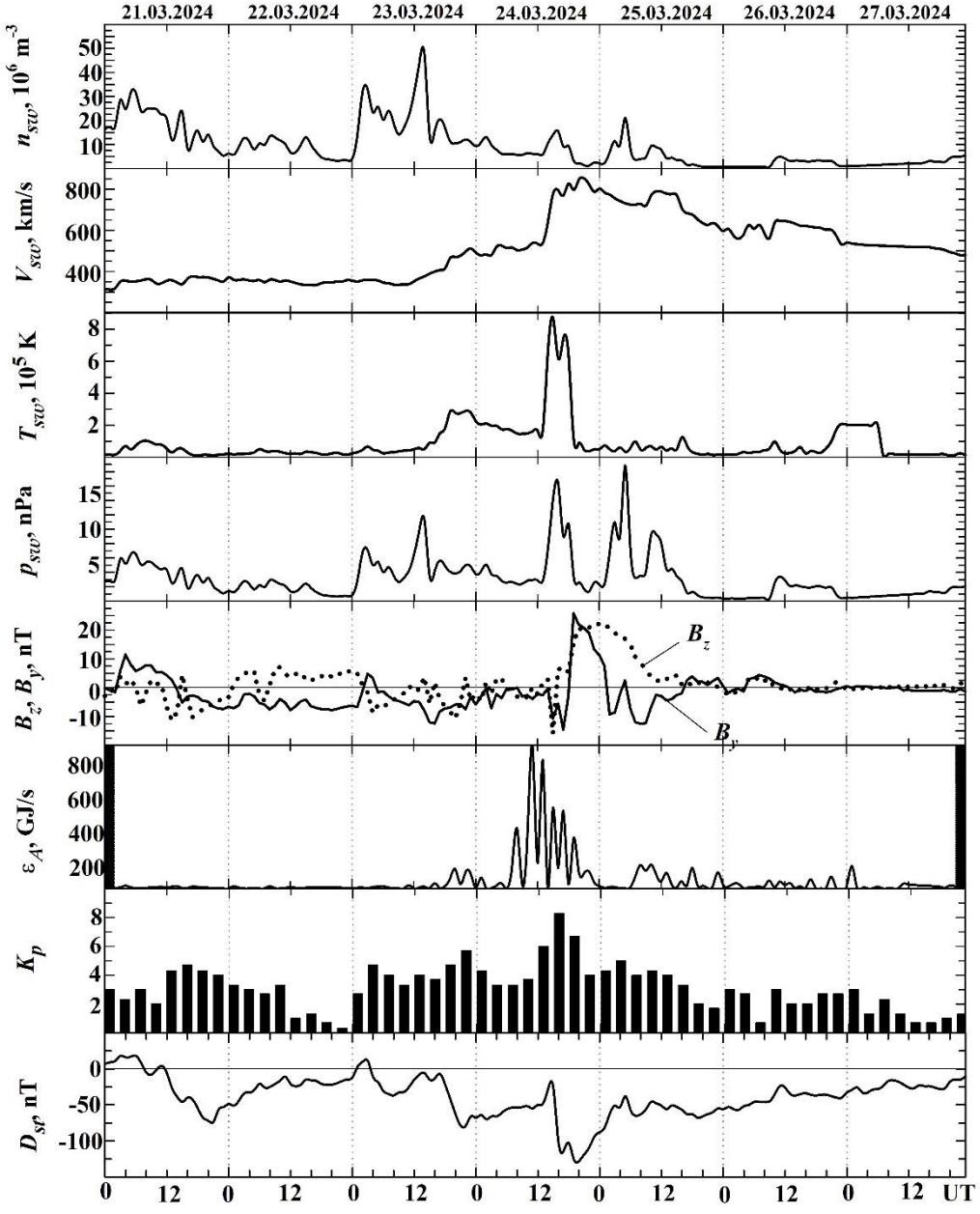

Figure 2. UT variations in the solar wind parameters: measured proton number density, n_{sw}, radial plasma flow speed V_{sw}, plasma temperature T_{sw}, calculated dynamic pressure p_{sw}, measured B_z and B_y components of the interplanetary magnetic field; calculated energy, ε_A, transferred from the solar wind into the Earth's magnetosphere per unit time; K_p and D_{st} indices (retrieved from OMNI2 database https://omniweb.gsfc.nasa.gov/form/dx1.html) for the March 21–27, 2024, period.

https://doi.org/10.5194/egusphere-2025-4375
Preprint. Discussion started: 17 September 2025

The solar wind plasma temperature T_{sw} exhibits the following behavior. The temperature T_{sw} shows fluctuations within ~10^4–10^5 K until the middle of the day on March 23, 2024. After 15:00 UT on March 23, 2024, it exhibits an increase from ~5×10^4 K to 3×10^5 K over 5 h in duration. The next, most significant, enhancement in T_{sw} to 8.7×10^5 K occurs from 13:00 UT to 19:00 UT on March 24, 2024. The last noticeable increase of T_{sw} is observed during the night of March 26/27, 2024, when T_{sw} does not exceed 2.2×10^5 K.

The calculated dynamic pressure, p_{sw}, of the solar wind gives the main contribution to the energetics of the geospace storm. In total, seven enhancements are noticeable in p_{sw}. The first occurs on March 21, 2024, and has a maximum of 7 nPa. Two others are smaller than 8 nPa and 12 nPa and arise on March 23, 2024, while on March 24, 2024, a maximum value of p_{sw} reaches ~17 nPa during approximately 7 h. The greatest increase of up to 18.6 nPa is observed on March 25, 2024, and persists for about 6 h; on the same day, a weaker enhancement of p_{sw} is less than 9 nPa and lasts for ~4 h. The final increase in p_{sw} of up to 3–4 nPa occurs on March 26, 2024.

The north-south component of the interplanetary magnetic field (IMF) B_z exhibits five southward turnings: two turnings on both March 21, 2024, and March 23, 2024, and one, the strongest, on March 24, 2024, with $B_{z\min} \approx -15.8$ nT. On the same day, the northward directed IMF shows a maximum of $B_{z\max} \approx 22.3$ nT. The B_y component strength of the IMF varies from –14.5 nT to 25.8 nT. It should be noted that the B_z component strength shows minute variations on March 25, 2024.

Akasofu's epsilon parameter, ε_A, which characterizes the energetics of the magnetospheric storm, shows the greatest and numerous (up to five) increases on March 24, 2024, when it changes from 380 GJ/s to a maximum of $\varepsilon_{A\max} \approx 1000$ GJ/s. On March 23 and 25, 2024, its values are 120–180 GJ/s, whereas the value of ε_A does not exceed ~1 GJ/s on March 21, 2024.

The K_p index shows five increases: on March 21, 2024, up to 5_-; on March 23, 2024, up to 5_- and 5 in the first and second half of day, respectively; on March 24, 2024, up to 8_+; and on March 25, 2024, up to 4.

The D_{st} index also exhibits five decreases: on March 21, 2024, down to –75 nT; on March 23, 2024, down to –35 nT and –76 nT; on March 24, 2024, down to –128 nT; and on March 25, 2024, down to –64 nT.

Thus, one has a valid reason to consider the geospace storm, as well as the geomagnetic storm, a multistep (repeatable) storm that occurred during March 21–25, 2024.

4 Analysis results

The temporal variations in the northward *X*-, eastward *Y*-, and vertical *Z*-component of the geomagnetic field strengths observed during March 21–27, 2024, are considered in the eastern (Fig. A1–A8) and western (Fig. B1–B8) hemispheres separately.

4.1 Eastern hemisphere

The repeatable geomagnetic storms are appropriate to consider by date (Table 3).

https://doi.org/10.5194/egusphere-2025-4375
Preprint. Discussion started: 17 September 2025

Table 3. Peak-to-peak amplitude of variations in a geomagnetic field strength at the eastern hemisphere stations during March 21–25, 2024.

Station	Component	March 2024				
		21–22	23	23–24	24	25
HRN	*X*	400	200	600	1300	300
	Y	300	180	180	900	300
	Z	200	200	500	925	450
PET	*X*	75	30	100	235	70
	Y	100	50	100	190	60
	Z	40	20	60	150	10
KHB	*X*	80	20	100	250	50
	Y	80	90	70	105	60
	Z	20	25	35	40	20
GUA	*X*	170	210	110	130	120
	Y	40	30	45	65	15
	Z	40	30	30	65	20
KDU	*X*	150	150	70	180	100
	Y	60	90	70	70	70
	Z	55	60	35	35	35
CTA	*X*	90	120	50	175	100
	Y	70	110	90	90	90
	Z	65	40	30	30	25
CNB	*X*	70	45	75	180	100
	Y	110	100	100	140	100
	Z	30	35	35	55	30
MCQ	*X*	600	400	400	1700	300
	Y	400	120	200	1500	100
	Z	550	300	200	1000	200

4.1.1 Geomagnetic storm of March 21, 2024

At the high-latitude HRN station (Fig. A1), the storm commences in the second half of March 21, 2024, and continues until ~12:00 UT on March 21, 2024. The maximum peak-to-peak amplitude of variations in the *X*-, *Y*-, and *Z*-components of a geomagnetic field strength is 400 nT, 300 nT, 200 nT, respectively.

https://doi.org/10.5194/egusphere-2025-4375
Preprint. Discussion started: 17 September 2025

At the other seven stations in the eastern hemisphere, the geomagnetic storm occurs at night, in the daytime, and again at night. At the middle latitude PET station (Fig. A2), the peak-to-peak amplitude of variations in the *X*-, *Y*-, and *Z*-components of a geomagnetic field strength attains 75 nT, 100 nT, and 40 nT, respectively. At another middle latitude KHB station (Fig. A3), the peak-to-peak amplitude does not exceed 80 nT, 80 nT, and 20 nT, respectively. At low-latitude GUA, KDU, and CTA stations (Figs. A4–A6), the peak-to-peak amplitude attains 170 nT, 40 nT, 40 nT; 150 nT, 60 nT, 50 nT; and 90 nT, 70 nT, 65 nT, respectively. At the middle latitude CNB station (Fig. A7) and high latitude MCQ station (Fig. A8), the peak-to-peak amplitude is 70 nT, 110 nT, and 30 nT; as well as 600 nT, 400 nT, and 550 nT, respectively.

4.1.2 First geomagnetic storm of March 23, 2024

At the high-latitude HRN station (Fig. A1) in the daytime, the peak-to-peak amplitude of variations in the *X*-, *Y*-, and *Z*-components of a geomagnetic field strength is 200 nT, 180 nT, and 200 nT, respectively. At the rest of the stations, the storm occurs at night and in the evening hours. At the mid-latitude PET and KHB stations (Figs. A2 and A3), the peak-to-peak amplitude attains 30 nT, 50 nT, 20 nT, and 20 nT, 90 nT, 25 nT, respectively. At the low-latitude GUA, KDU, and CTA stations (Figs. A4–A6), the maximum peak-to-peak amplitude is about 210 nT, 30 nT, 30 nT; 150 nT, 90 nT, 60 nT; as well as 120 nT, 110 nT, 40 nT, respectively. At mid-latitude CNB and high latitude MCQ stations in the southern hemisphere (Figs. A7 and A8), the peak-to-peak amplitude does not exceed 45 nT, 100 nT, 35 nT and 400 nT, 120 nT, 300 nT, respectively.

4.1.3 Second geomagnetic storm of March 23–24, 2024

This storm commences in the second half of March 23, 2024, and continues through the remainder of March 23, 2024, and until approximately 13:00 UT on March 24, 2024. At the high-latitude HRN station (Fig. A1), the peak-to-peak amplitude of variations in the *X*-, *Y*-, and *Z*-components of a geomagnetic field strength attains 600 nT, 180 nT, and 500 nT, respectively. At middle latitude PET and KHB stations (Figs. A2 and A3), the peak-to-peak amplitude is smaller than 100 nT, 100 nT, 60 nT, and 100 nT, 70 nT, 35 nT, respectively. At low latitude GUA, KDU, and CTA stations (Figs. A4–A6), the peak-to-peak amplitude is within the limits 110 nT, 45 nT, 30 nT; 70 nT, 70 nT, 35 nT; as well as 50 nT, 90 nT, 30 nT, respectively. At middle latitude CNB and high latitude MCQ stations (Figs. A7 and A8), the peak-to-peak amplitude attains 75 nT, 100 nT, 35 nT, and 400 nT, 400 nT, 200 nT, respectively.

4.1.4 Main geomagnetic storm of March 24, 2024

This storm commences in the second half of March 24, 2024, and continues to 05:00 UT on March 25, 2024. At the high latitude HRN station (Fig. A1), the peak-to-peak amplitude of variations in the *X*-, *Y*-, and *Z*-components of a geomagnetic field strength is within the limits 1300 nT, 900 nT, and 925 nT, respectively. At the rest of the stations in the eastern hemisphere, the storm's main phase occurs during the night. At mid-latitude PET and KHB stations (Figs. A2 and A3), the peak-to-peak amplitude is about 235 nT, 190 nT, 150 nT, and 250 nT, 105 nT, 40 nT, respectively. At the low-latitude GUA,

https://doi.org/10.5194/egusphere-2025-4375
Preprint. Discussion started: 17 September 2025

KDU, and CTA stations (Figs. A4–A6), the peak-to-peak amplitudes are seen to be 130 nT, 65 nT, 65 nT; 180 nT, 70 nT, 35 nT; as well as 175 nT, 90 nT, 30 nT, respectively. At the middle latitude CNB (Fig. A7) and high latitude MCQ (Fig. A8) stations, the peak-to-peak amplitude attains 180 nT, 140 nT, 55 nT and 1700 nT, 1500 nT, 1000 nT, respectively.

4.1.5 Geomagnetic storm of March 25, 2024

This storm commences at ~05:00 UT on March 25, 2024, and persists for more than 27 h. At the high latitude HRN station (Fig. A1), the peak-to-peak amplitude of variations in the *X*-, *Y*-, and *Z*-components of a geomagnetic field strength is 300 nT, 300 nT, 450 nT, respectively. At the middle latitude PET and KHB stations (Figs. A2 and A3), the peak-to-peak amplitude attains 70 nT, 60 nT, 10 nT, and 50 nT, 60 nT, 20 nT, respectively. At the low latitude GUA, KDU, and CTA stations (Figs. A4–A6), the peak-to-peak amplitude is within the limits 120 nT, 15 nT, 20 nT; 100 nT, 70 nT, 35 nT; and 100 nT, 90 nT, 25 nT, respectively. At the middle latitude CNB (Fig. A7) and high latitude MCQ (Fig. A8) stations in the southern hemisphere, the peak-to-peak amplitude does not exceed 100 nT, 100 nT, 30 nT, and 300 nT, 100 nT, 200 nT, respectively.

4.2 Western hemisphere

The repeatable geomagnetic storms are considered by date (Table 4).

4.2.1 Geomagnetic storm of March 21, 2024

At all stations in the western hemisphere, the storm commences during the day on March 21, 2024, and ceases during the day on March 22, 2024. At the high latitude THL, GDH, IQA, and BLC stations (Figs. B1–B4), the peak-to-peak amplitude of variations in the *X*-, *Y*-, and *Z*-components of a geomagnetic field strength attains 300 nT, 200 nT, 120 nT; 200 nT, 200 nT, 350 nT; 200 nT, 250 nT, 400 nT; and 300 nT, 200 nT, 500 nT, respectively. At the middle latitude STJ and SBL stations (Figs. B5 and B6) the peak-to-peak amplitude is about 120 nT, 110 nT, 100 nT and 100 nT, 20 nT, 65 nT, respectively. At the low latitude VSS station (Fig. B7), the peak-to-peak amplitude does not exceed 100 nT, 60 nT, 40 nT, respectively. At the high latitude AIA station in the southern hemisphere (Fig. B8), the peak-to-peak amplitude attains 110 nT, 160 nT, 90 nT, respectively.

4.2.2 First geomagnetic storm of March 23, 2024

At all the stations in the western hemisphere, this storm occurs at night, in the morning hours, and during the day. At the high latitude THL, GDH, IQA, and BLC stations (Figs. B1–B4), the peak-to-peak amplitude of variations in the *X*-, *Y*-, and *Z*-components of a geomagnetic field strength is in the limits 200 nT, 50 nT, 50 nT; 50 nT, 100 nT, 400 nT; 300 nT, 300 nT, 280 nT; and 100 nT, 240 nT, 500 nT, respectively. At the mid-latitude STJ and SBL stations (Figs. B5 and B6), the peak-to-peak amplitude is 50 nT, 110 nT, 80 nT and 70 nT, 20 nT, 20 nT, respectively. At the low latitude VSS station (Fig. B7), the

https://doi.org/10.5194/egusphere-2025-4375
Preprint. Discussion started: 17 September 2025

peak-to-peak amplitude is smaller than 50 nT, 20 nT, 5 nT, respectively. At the high latitude AIA station in the southern hemisphere (Fig. B8), the peak-to-peak amplitude attains 80 nT, 70 nT, 110 nT, respectively.

Table 4. Peak-to-peak amplitude of variations in a geomagnetic field strength at the western hemisphere stations during March 21–25, 2024.

Station	Component	March 2024				
		21–22	23	23–24	24	25
THL	*X*	300	200	350	900	150
	Y	200	50	200	1500	200
	Z	120	50	150	1300	300
GDH	*X*	200	50	350	1700	200
	Y	200	100	200	1100	200
	Z	350	400	550	900	350
IQA	*X*	200	300	100	2300	200
	Y	250	300	250	1600	200
	Z	450	280	450	1200	150
BLC	*X*	300	100	300	1600	200
	Y	200	240	200	950	200
	Z	500	500	700	1750	200
STJ	*X*	120	50	80	290	80
	Y	110	110	110	240	120
	Z	100	80	110	300	20
SBL	*X*	100	70	120	360	70
	Y	20	20	20	35	20
	Z	65	20	100	130	30
VSS	*X*	100	50	220	300	130
	Y	60	20	70	75	70
	Z	40	5	55	95	50
AIA	*X*	110	80	60	190	140
	Y	160	70	200	220	60
	Z	90	110	160	150	50

4.2.2 Second geomagnetic storm of March 23–24, 2024

This storm persists for about one day. At the high latitude THL, GDH, IQA, and BLC stations (Figs. B1–B4), the peak-to-peak amplitude of variations in the *X*-, *Y*-, and *Z*-components of a geomagnetic field strength is about 350 nT, 200 nT, 150

https://doi.org/10.5194/egusphere-2025-4375
Preprint. Discussion started: 17 September 2025

nT; 350 nT, 200 nT, 550 nT; 300 nT, 250 nT, 450 nT; and 300 nT, 200 nT, 700 nT, respectively. At the middle latitude STJ and SBL stations (Figs. B5 and B6), the peak-to-peak amplitude does not exceed 80 nT, 110 nT, 110 nT and 120 nT, 20 nT, 100 nT, respectively. At the low latitude VSS station (Fig. B7), the peak-to-peak amplitude is in the limits 220 nT, 70 nT, 55 nT. At the high latitude AIA station in the southern hemisphere (Fig. B8), the peak-to-peak amplitude attains 60 nT, 200 nT, 170 nT, respectively.

4.2.3 Main geomagnetic storm of March 24, 2024

This storm persists for about 15 h with the commencement at about 14:00 UT on March 24, 2024. The peak-to-peak amplitude of variations in the *X*-, *Y*-, and *Z*-components of a geomagnetic field strength at the high latitude THL, GDH, IQA, and BLC stations (Figs. B1–B4), attains 900 nT, 1500 nT, 1300 nT; 1700 nT, 1100 nT, 900 nT; 2300 nT, 1600 nT, 1200 nT; 1600 nT, 950 nT, 1750 nT, respectively. At the middle latitude STJ and SBL stations (Figs. B5 and B6), the peak-to-peak amplitude does not exceed 290 nT, 240 nT, 300 nT, and 360 nT, 35 nT, 130 nT. At the low latitude VSS station (Fig. B7), the peak-to-peak amplitude is in the limits 300 nT, 75 nT, 95 nT. At the high latitude AIA station in the southern hemisphere (Fig. B8), the peak-to-peak amplitude is 190 nT, 220 nT, 150 nT, respectively.

4.2.4 Geomagnetic storm of March 25, 2024

This storm, persisting for more than a day, occurs at the stations in the western hemisphere both at night and in the daytime. At the high latitude THL, GDH, IQA, and BLC stations (Figs. B1–B4), the peak-to-peak amplitude of variations in the *X*-, *Y*-, and *Z*-components of a geomagnetic field strength is close to 150 nT, 200 nT, 300 nT; 200 nT, 200 nT, 350 nT; 200 nT, 200 nT, 150 nT; and 200 nT, 200 nT, 200 nT, respectively. At the middle latitude STJ and SBL stations (Figs. B5 and B6), the peak-to-peak amplitude is in the limits 80 nT, 120 nT, 20 nT and 70 nT, 20 nT, 30 nT. At the low latitude VSS station (Fig. B7), the peak-to-peak amplitude is 130 nT, 70 nT, 50 nT. At the high latitude AIA station (Fig. B8), which is in the southern hemisphere, the peak-to-peak amplitude is 140 nT, 60 nT, 50 nT, respectively.

5 Results of calculations of the energetics of the storms

The energetics of the geospace, magnetospheric, and geomagnetic storms is considered separately.

5.1 Energetics of the geospace storm

The fast solar wind flow exerts the dynamic pressure p_{sw}, the magnetic pressure p_m, and the kinetic pressure p_k, with the solar dynamic pressure being the greatest, and which is assumed to be dominant in driving a geospace storm. The power of the solar wind dynamic pressure is given by the following relation (Chernogor, 2025b, 2025c):

$$P_{sw} = p_{sw} S_{m0} V_{sw}. \quad (1)$$

https://doi.org/10.5194/egusphere-2025-4375
Preprint. Discussion started: 17 September 2025

Here, $S_{m0} \approx 1.28 \times 10^6$ m^2 is the surface area of the magnetosphere cross section calculated assuming that its radius is 10 Earth's radii, R_E, V_{sw} is the solar wind speed. Over the interval, ΔT_{sw}, of increased solar wind dynamic pressure, the energy supplied to the geospace medium is estimated from:

$$E_{sw} \approx \frac{1}{2} P_{sw} \Delta T_{sw} . \quad (2)$$

Table 5 presents the results of calculations of P_{sw} and E_{sw} from Eqs. (1) and (2) for all five increases in the dynamic pressure that occurred over March 21–25, 2024. The interesting results shown in this table are that the variations in p_{sw} from 7 nPa to 19 nPa and in the solar wind speed from 320 km s^{-1} to 800 km s^{-1} lead to an increase in the power P_{sw} from 29 TW to 192 TW, and when multiplied by the corresponding values of ΔT_{sw}, these lead to a variation in the energy transferred into the geospace medium from 0.73 EJ to 2.8 EJ.

Table 5. Salient parameters of the repeating geomagnetic storm of March 21–25, 2024, energetics.

Storm parameter or characteristic	March 21	March 23	March 23	March 24	March 25
Solar wind dynamic pressure (nPa)	7	8	13	17	19
Solar wind speed (km s^{-1})	320	320	300	800	800
β of the plasma	0.75	0.61	1.25	0.52	0.24
Power of the geospace storm (TW)	29	33	50	174	192
Energy of the geospace storm (EJ)	0.73	0.59	0.36	2.5	2.8
Duration of the geospace storm (h)	14	10	4	8	8
Power of the magnetospheric storm (GJ/s)	13	13	130	1000	190
Energy of the magnetospheric storm (TJ)	90	90	1360	22000	2000
Duration of the magnetospheric storm (h)	4	4	6	12	6
Maximum power of the geomagnetic storm (GW)	93	97	208	283	89
Energy of the geomagnetic storm (PJ)	3	1.4	3	5.1	4.5
Duration of the geomagnetic storm's main phase (h)	9	4	4	5	14
$K_{p\max}$	5–	5	6	8+	4
$D_{st\min}$ (nT)	–75	–35	–76	–128	–64
Description	G1, minor	G1, minor	G2, moderate	G4, severe	G0, very minor

5.2 Energetics of the magnetospheric storm

The energetics of the magnetospheric storm is determined by the magnetic p_m and kinetic p_k pressures, which are defined as

$$p_m = \frac{B^2}{2\mu_0},$$

https://doi.org/10.5194/egusphere-2025-4375
Preprint. Discussion started: 17 September 2025

$$p_k = k\,T_{sw}\,n_{sw},$$

where B is the magnetic field induction in the interplanetary space, μ_0 is the permeability of free space, and k is Boltzmann's constant. The relative effectiveness of the magnetic and kinetic pressures is estimated by calculating the ratio of the kinetic and magnetic pressures, which is called the β of the plasma

$$\beta = \frac{p_k}{p_m} = 2\mu_0 \frac{kT_{sw}n_{sw}}{B^2}\,. \tag{3}$$

Table 5 presents results of estimating the β of the plasma from Eq. (3), which show that β ≈ 0.24–1.25.

The magnetic pressure corresponds to the power determined from Akasofu's parameter (Akasofu, 1966)

$$\varepsilon_A = 8\pi R_{ef}^2\, p_m V_{sw} \sin^4(\theta/2)\,, \tag{4}$$

where $R_{ef} \approx 7R_E$ is the effective radius of the magnetosphere, $\theta = \arctan(B_y/B_z)$, the angle θ varies from $-\pi/2$ to $\pi/2$, and $\sin^4(\theta/2)$ is in the range 0–0.25. If the duration of an increase in ε_A is ΔT_m, then the energy of the magnetic pressure is given by

$$E_A = \frac{1}{2}\varepsilon_{A\max}\Delta T_m\,. \tag{5}$$

where ε_{Amax} is the maximum ε_A. The estimates of ε_A and E_A from Eqs. (4) and (5) are also presented in Table 5, from which it follows that ε_A varies within the limits 13–1000 GJ/s, and the energy varies from 90 TJ to 22 PJ. The energy of the kinetic pressure is also approximately of the same order of magnitude.

As expected, the energetics of the dynamic pressure is significantly superior to the energetics of the magnetic and kinetic pressures.

5.3 Energetics of the geomagnetic storm

The following relation can be used conveniently to estimate the energy of the geomagnetic storm (Gonzalez et al., 1994):

$$E_{ms} = \frac{3}{2}E_{md}\frac{\left|D_{st}^*\right|}{B_0}\,, \tag{6}$$

where $E_{md} = 0.8$ EJ is the total energy of the Earth's dipole magnetic field, $B_0 = 3 \times 10^{-5}$ T is the Earth's magnetic induction at the equator, D_{st}^* is a corrected D_{st} given by the relation

$$D_{st}^* = D_{st} - bp_{sw}^{1/2} + c\,,$$

where $b = 5 \times 10^5$ nT Pa$^{1/2}$, $c = 20$ nT, and p_{sw} is in Pa.

The maximum power of the geomagnetic storm is given by

$$P_{ms} = \frac{E_{ms}}{\Delta T_{ms}}\,, \tag{7}$$

where ΔT_{ms} is the duration of the geomagnetic storm's main phase.

https://doi.org/10.5194/egusphere-2025-4375
Preprint. Discussion started: 17 September 2025

The results of calculations of the energy and power of the geomagnetic storms from Eqs. (6) and (7) are also given in Table 5, from which it follows that E_{ms} varies in the limits 1.4–5.1 PJ, and the power varies from 93 GW to 283 GW.

6 Discussion

6.1 Sources of and physical mechanisms for repeating geomagnetic storms

As can be seen in Fig. 2, the five geomagnetic storms of March 21–22, 2024; March 23, 2024; March 23–24, 2024; March 24–25, 2024; and March 25–26, 2024, were preceded by increases in the solar wind dynamic pressure of up to 7 nPa, 8 nPa, 12 nPa, 17 nPa, 19 nPa, and 10 nPa respectively. Moreover, the main storm of March 24–25, 2024, was preceded by increases in the solar wind speed of up to 800 km s^{-1}, plasma temperature of up to 8.7×10^5 K, and in Akasofu's parameter of up to 1000 GJ s^{-1}. The solar wind structures with enhanced n_{sw}, V_{sw}, and $|B_z|$ are known as sheaths (Kilpua et al., 2017). Such structures are described in a series of studies (Palmerio et al., 2016; Myllys et al., 2016; Lugaz et al., 2015, 2017; Manchester et al., 2017; Chernogor, 2025a). The sheaths lead to multi-step geomagnetic storms, and the geomagnetic storm of April 23–24, 2023, is an example of a two-step geomagnetic storm caused by the shock sheath and the magnetic cloud in the CME **(**Ghag et al., 2024; Chernogor, 2025a). One has a valid reason to consider that all five storms are due to increases in n_{sw}, V_{sw}, and p_{sw}, i.e., due to sheaths in the solar wind.

Indeed, the storm of March 21–22, 2024, was preceded by an enhancement in n_{sw} of up to 3.3×10^7 m^{-3}, and by a decrease in B_z down to –11 nT. The solar wind proton density increased from 3×10^6 m^{-3} to 3.5×10^7 m^{-3}, and the IMF B_z decreased from 5 nT to –10 nT, prior to the storm of March 23, 2024. Before the storm of March 23–24, 2024, the solar wind proton density increased up to 4.8×10^7 m^{-3} and the IMF B_z decreased from 3 nT to –10 nT; however, the solar wind proton density increased only to 1.5×10^7 m^{-3}, and the IMF B_z reduced from 4 nT up to –15.8 nT prior to the second, main storm of March 24, 2024. The solar wind proton density increased up to 2×10^7 m^{-3}, and the IMF B_z decreased from 20 nT to 2 nT prior to the storm of March 25–26, 2024; the greatest (up to 19 nPa) increases in p_{sw} were noted during this period. It should be noted that the greatest increases in V_{sw} and T_{sw} occurred prior the main storm of March 24, 2024. Apparently, this storm was due to high-speed solar wind plasma streams. Also, the storm of March 25, 2024, was different from the other 4 storms in that the IMF $B_z > 0$ nT.

6.2 Comparative analysis of the geomagnetic storms of March 2024

The magnetometer stations in the eastern (Table 3) and western (Table 4) hemispheres are considered separately.

6.2.1 Eastern hemisphere

The first general feature is that the greatest peak-to-peak amplitude of variations in the geomagnetic field strength is most often inherent in the *X* component, whereas the smallest one is observed in the *Z* component.

https://doi.org/10.5194/egusphere-2025-4375
Preprint. Discussion started: 17 September 2025

At the majority of the stations during the storm of March 21–22, 2024, the peak-to-peak amplitude was greater than that during the first storm of March 23, 2024. This pattern is disrupted at the low latitude GUA and KDU stations. The intensity of March 23–24, 2024, storm is comparable to that of the storm of March 21–22, 2024. The storm of March 24, 2024, was the greatest, when the peak-to-peak amplitude of variations in the geomagnetic field strength exceeded that observed during March 21–23, 2024 by a factor of a few times. The storm of March 25, 2024, was somewhat weaker than the storm of March 21–22, 2024.

6.2.2 Western hemisphere

At the stations in the western hemisphere the peak-to-peak amplitude of variations in the *X* component strength was not always the greatest, and the peak-to-peak amplitude of variations in the *Z* component strength was not the smallest one. Often, at the high latitude stations, the peak-to-peak amplitude of the *Z* component was greater than the peak-to-peak amplitude of the *Y* component and even than that of the *X* component.

The peak-to-peak amplitude during the first storm of March 23, 2024 was smaller than that during the storm of March 21–22, 2024, while the March 21–22, 2024, and March 23–24, 2024, storm intensities were comparable. At the same time, the peak-to-peak amplitude during March 24, 2024, exceeded the peak-to-peak amplitude during March 21–22, 2024, by a factor of 2–10, whereas the intensity of the March 21–22, 2024, and March 25, 2024, storms were comparable.

Generally, the peak-to-peak amplitude of variations in all components of the geomagnetic field strength in the western hemisphere was greater than that in the eastern hemisphere. Most of the storm time of all geomagnetic storms in the eastern hemisphere occurred at night and in the morning hours, whereas in the western hemisphere all geomagnetic storms, except for the storm of March 23, 2024, occurred during the course of a day. The electron density in the daytime ionosphere is greater than that in the nighttime ionosphere, and the ionospheric electric currents are greater, which determines the geomagnetic effect. The ionospheric currents explain the decrease in the peak-to-peak amplitude during the first storm of March 23, 2024 compared to the peak-to-peak amplitude during March 21–22, 2024.

6.3 Intercomparison of the energetics of the geomagnetic storms of March 21–25, 2024

Table 5 presents the results of the calculations of the energetics of the geospace, magnetospheric, and geomagnetic storms observed during March 21–25, 2024, which show that the storms of March 21, 23, 23, 24, and 25, 2024, correspond to the geomagnetic K_p index attaining 5_-, 5, 6, 8_+, and 4, respectively, and to minimum D_{st} values of –75 nT, –35 nT, –76 nT, –128 nT, –64 nT, respectively. They correspond to a minor G1-class geomagnetic storm, a minor G1-class geomagnetic storm, a moderate G2-class geomagnetic storm, a severe G4-class geomagnetic storm, and a very minor G0-class geomagnetic storm, respectively. The power and energy of the geospace storms caused by solar wind dynamic pressure enhancements are 29 TW, 33 TW, 50 TW, 174 TW, 192 TW and 0.73 EJ, 0.59 EJ, 0.36 EJ, 2.5 EJ, 2.8 EJ, respectively. The power and energy of the magnetospheric storms caused by increases in the interplanetary magnetic pressure are 13 GJ/s, 13 GJ/s, 130 GJ/s, 1000

https://doi.org/10.5194/egusphere-2025-4375
Preprint. Discussion started: 17 September 2025

GJ/s, 190 GJ/s and 90 TJ, 90 TJ, 1360 TJ, 22,000 TJ, and 2000 TJ, respectively. Maximum power and energy of the geomagnetic storms attain 93 GW, 97 GW, 208 GW, 283 GW, 89 GW and 3 PJ, 1.4 PJ, 3 PJ, 5.1 PJ, 4.5 PJ, respectively.

Consequently, one has a valid reason to consider the geomagnetic storm that commenced at about 14:00 UT on March 24, 2024, the main storm in March 2024, and the weaker disturbances of March 25–26, 2024, being superimposed upon it. In total, this storm persisted for more than 3 days.

6.4 Main geomagnetic storm of March 2024

The limits of variations in the strength of the *X*-, *Y*-, and *Z*-components during the main geomagnetic storm that commenced on March 24, 2024, are considered separately in the eastern and western hemispheres.

6.4.1 Eastern hemisphere

Table 6 shows that the background variations in the peak-to-peak amplitude in the eastern hemisphere occur in the range from ±5 nT to ±50 nT, whereas the strength variations increase by a factor of a few times to a few tens of times on March 24, 2024. Generally, the *X* component variations are the greatest, and the peak-to-peak amplitude exceeds 1000 nT at the HRN and MCQ stations.

Table 6. Limits of variations in the geomagnetic field strength at the stations in the eastern hemisphere on March 24, 2024.

Station	Background (nT)			Disturbance on March 24, 2024 (nT)		
	X component	*Y* component	*Z* component	*X* component	*Y* component	*Z* component
HRN	–25	–20	–25	–1000	–500	–525
	25	20	25	300	400	410
PET	–25	–20	–10	–75	–60	–125
	25	20	10	160	130	25
KHB	–10	–10	–10	–90	–40	–25
	10	10	10	160	65	15
GUA	–15	–15	–10	–80	–35	–35
	15	15	10	50	30	30
KDU	–30	–20	–10	–90	–40	–25
	30	20	10	90	30	10
CTA	–10	–30	–10	–75	–45	–10
	10	30	20	100	45	20
CNB	–20	–40	–5	–50	–90	–15
	20	40	5	130	50	40
MCQ	–30	–40	–50	–1400	–1400	–500
	30	40	50	300	100	500

Table 7 shows the disturbed-to-quiet time ratios of the peak-to-peak amplitude of variations in the geomagnetic field strength during the March 24, 2024, storm at the stations in the eastern hemisphere. The maximum peak-to-peak

https://doi.org/10.5194/egusphere-2025-4375
Preprint. Discussion started: 17 September 2025

amplitude of variations occurred at the high latitude HRN and MCQ stations, whereas the minimum variations (a factor of 1.8–3) were noted at the low latitude KDU station.

Table 7. Disturbed-to-quiet time ratios of the maximum peak-to-peak amplitude of variations in the geomagnetic field strength during the March 24, 2024, storm in the eastern hemisphere.

Station	*X* component	*Y* component	*Z* component
HRN	26	22.5	18.7
PET	4.7	4.8	7.5
KHB	12.5	5.3	2
GUA	4.3	2.2	3.3
KDU	3	1.8	1.8
CTA	8.8	1.5	1
CNB	4.5	1.8	5.5
MCQ	28.3	18.8	10

6.4.2 Western hemisphere

The background variations in the strength lies in the range ±10 nT to ±100 nT, i.e., they are noticeably greater than those in the eastern hemisphere, as can be seen from Table 8. The peak-to-peak amplitude of the variations on March 24, 2024, at high latitude stations attained ~1000–2000 nT. At the other stations the peak-to-peak amplitude remained within ~100–300 nT.

The maximum disturbed-to-quiet time ratios of the peak-to-peak amplitude of variations in the geomagnetic field strength during March 24, 2024, storm in the western hemisphere are presented in Table 9, which show that the maximum values of the *X*-, *Y*-, and *Z*-components changed by a factor of 3.2–23, 1.9–18.8, and 4.8–15, respectively.

6.5 Latitudinal dependence of storm intensity

The peak-to-peak amplitude of variations in the *X*-, *Y*-, and *Z*-components of a geomagnetic field strength shows a clear tendency to increase with increasing latitude during all the storms under consideration.

In the eastern hemisphere, the peak-to-peak amplitude usually varies from a few tens of nano teslas to ~200 nT at the low latitude stations, is almost the same at the middle latitude stations, and attains a few hundred to 1500–1700 nano teslas at the high latitude stations.

It should be noted that the geographic latitude of the MCQ station is close to 55°S, whereas its geomagnetic latitude is ~–59° (Table 3), therefore this station should be considered a rather high-latitude one.

The peak-to-peak amplitude does not exceed 300 nT at the low latitude VSS station in the western hemisphere. Almost the same peak-to-peak amplitudes (up to ~300–360 nT) are at the middle latitude stations, whereas the peak-to-peak

https://doi.org/10.5194/egusphere-2025-4375
Preprint. Discussion started: 17 September 2025

amplitude is ~1000–2300 nT at the high latitude stations in the northern hemisphere (Table 4). Only at the AIA station in the southern hemisphere, the peak-to-peak amplitude is within ~50–200 nT. It should be remarked that the geographic latitude of the AIA station is close to 65°S, whereas its geomagnetic latitude is approximately 56°S (Table 2). This means that this station is rather a mid-latitude station in terms of geomagnetic coordinates.

415

Table 8. Limits of variations in the geomagnetic field strength at the stations in the western hemisphere on March 24, 2024.

Station	Background (nT)			Disturbance on March 24, 2024 (nT)		
	X component	*Y* component	*Z* component	*X* component	*Y* component	*Z* component
THL	–40	–40	–50	–550	–750	–600
	40	40	50	350	750	700
GDH	–50	–50	–80	–1200	–300	–500
	50	50	80	500	800	400
IQA	–50	–50	–100	–1600	–550	–800
	50	50	100	700	1050	400
BLC	–50	–30	–60	–900	–200	–750
	50	30	60	700	750	1000
STJ	–10	–10	–10	–210	–160	–150
	10	10	10	80	80	150
SBL	–20	–5	–10	–260	–20	–90
	20	5	10	100	15	40
VSS	–10	–20	–10	–110	–35	–45
	10	20	10	190	40	50
AIA	–30	–30	–10	–150	–110	–50
	30	30	10	40	110	100

Table 9. Disturbed-to-quiet time ratios of the maximum peak-to-peak amplitude of variations in the geomagnetic field strength during the March 24, 2024, storm in the western hemisphere.

Station	*X* component	*Y* component	*Z* component
THL	11.3	18.8	12
GDH	17	11	5.6
IQA	23	16	6
BLC	16	15.8	14.6
STJ	14.5	12	15
SBL	9	3.5	6.5
VSS	15	1.9	4.8
AIA	3.2	3.7	7.5

https://doi.org/10.5194/egusphere-2025-4375
Preprint. Discussion started: 17 September 2025

There are a few reasons that explain the deviations from the latitudinal dependence described above. The first is related to the mechanisms of the magnetic effect. In the high and middle latitudes, the variations in the components of the geomagnetic field strength are due to variations in the electron density N and electric current density **j**, whereas at low latitudes, because of the variations in the ring current. The second reason is that the disturbances in N and **j** are distributed in longitude and latitude highly unevenly, which leads to some violation of the latitudinal and even longitudinal dependences of the magnetic effect. The other reason is the latitudinal dependence of electrodynamic processes, thermospheric winds, ionosphere-plasmasphere coupling, and ambipolar diffusion.

6.6 Intercomparison of the intense geomagnetic storms

The comparison includes the main storm of March 24–25, 2024, one of the strongest storms in solar cycle 25, the April 23–24, 2023 storm (Chernogor, 2025a, 2025b), the strongest storm of solar cycle 25, storm of May 10–11, 2024 (Chernogor, 2025c; Chernogor et al., 2025), and a super unique storm similar to the Carrington event of 1859 (Table 10).

Table 10. Salient parameters of severe, extreme, and super unique geomagnetic storms.

Storm parameter or characteristic	March 24, 2024	April 23–24, 2023	May 10–11, 2024	Super unique storm
$K_{p\max}$	8+	8+	9	11
$D_{st\min}$ (nT)	–128	–212	–412	<–1000
Power of the geospace storm (PW)	0.174	0.1	0.4	>10
Energy of the geospace storm (EJ)	2.5	1.8	6.5	>500
Duration of the geospace storm (h)	8	10	9	>30
Power of the magnetospheric storm (TJ/s)	1	2.8	15	>25
Energy of the magnetospheric storm (PJ)	22	50	82	>450
Duration of the magnetospheric storm (h)	12	10	3	10
Maximum power of the geomagnetic storm (TW)	0.28	0.67	1.4	>1.6
Energy of the geomagnetic storm (PJ)	5.1	9.7	20	>60
Duration of the geomagnetic storm's main phase (h)	5	4	4	10
Total storm duration	>120	>120	>120	>120
Description	G4, severe	G4, severe	G5, extreme	G7, Super-unique

These storms are described as Severe (G4), Severe (G4), Extreme (G5), and Super unique (G7), respectively, in terms of the NOAA geomagnetic storm classification augmented by the author. Maximum K_p indices and D_{st} minimum values for these storms are 8_+, 8_+, 9, 11 and –128 nT, –212 nT, –412 nT, and less than –1000 nT, respectively. The power and energy of the corresponding geospace storms are close to 0.17 PW, 0.1 PW, 0.4 PW, and more than 10 PW; 2.5 EJ, 1.8 EJ, 6.5 EJ, and more than 500 EJ, respectively. The energetics parameters of the magnetospheric storms are as follows: 1 TJ/s, 2.8 TJ/s, 15 TJ/s, and more than 25 TJ/s; 22 PJ, 50 PJ, 82 PJ, and more than 450 PJ, respectively. The geomagnetic storms have the

https://doi.org/10.5194/egusphere-2025-4375
Preprint. Discussion started: 17 September 2025

following energetics characteristics: 0.28 TW, 0.67 TW, 1.4 TW, and more than 1.6 TW; 5.1 PJ, 9.7 PJ, 20 PJ, and more than 60 PJ, respectively. The duration of these storms' main phase is about 5 h, 4 h, 4 h, and 10 h, respectively.

7 Conclusions

(1) The magnetic storm of March 21–26, 2024, is validated to be comprised of five storms, i.e., it is a multi-step storm, with the main storm occurring during March 24–25, 2024. A multi-step nature of this storm is unique to this event, and this storm is caused by isolated sheaths that appeared in the solar wind.

(2) The power of the geospace storms caused by increases in the solar wind dynamic pressure has been shown to be close to 29 TW, 33 TW, 50 TW, 174 TW, and 192 TW, and their energy does not exceed 0.73 EJ, 0.59 EJ, 0.36 EJ, 2.5 EJ, and 2.8 EJ.

(3) The power of the magnetospheric storms, caused by increases in the interplanetary magnetic pressure, has been demonstrated to be 13 GJ/s, 13 GJ/s, 130 GJ/s, 1000 GJ/s, and 190 GJ/s, and their energy to attain 90 TJ, 90 TJ, 1360 TJ, 22,000 TJ, and 2000 TJ. The energetics of the magnetic and kinetic pressures has been shown to be close to each other.

(4) The maximum power of the geomagnetic storms has been determined to be close to 93 GW, 97 GW, 208 GW, 283 GW, and 89 GW, and their energy to be smaller than 3 PJ, 1.4 PJ, 3 PJ, 5.1 PJ, and 4.5 PJ.

(5) The storms of March 21–22, 2024; March 23, 2024; March 23–24, 2024; March 24–25, 2024; and March 25–26, 2024, have been demonstrated to pertain to the storm classes G1 (minor), G1 (minor), G2 (moderate), G4 (severe), and G0 (very minor).

(6) In both the eastern and western hemispheres, the peak-to-peak amplitude of variations in a geomagnetic field strength exhibits a tendency to increase with increasing magnetic latitude. At high latitude stations, the peak-to-peak amplitude attains a maximum value of ~1000–2000 nT, whereas at mid- and low latitude stations they are observed to be within ~100–300 nT. The observed possible deviations from the tendency indicated above may be due to the different physical processes acting to cause variations in the geomagnetic field at high, middle, and low latitudes.

(7) The peak-to-peak amplitude of variations in a geomagnetic field strength has been shown to be the greatest during sunlit hours.

(8) The peak-to-peak amplitude of variations in a geomagnetic field strength during the storms is a factor of up to 23–28, 19–23, and 15–19 greater than that during quiet time reference period, in the northward *X*-, eastward *Y*-, and vertical *Z*-component of the geomagnetic field, respectively.

(9) The storm of March 24–25, 2024, termed the main storm, is the most intense of all five storms of March 21–26, 2024.

(10) The main storm of March 24–25, 2024, is comparable to the storm of April of 23–24, 2023, with respect to all its parameters. At the same time, it is less intense than the storm of May 10–11, 2024, the strongest storm of solar cycle 25, and even less intense than the Carrington event.

https://doi.org/10.5194/egusphere-2025-4375
Preprint. Discussion started: 17 September 2025

Appendix A

Here are presented the temporal variations in the strength of the *X*, *Y*, and *Z* components of the geomagnetic field during March 21–27, 2024, in the eastern hemisphere (Fig. A1–A8).

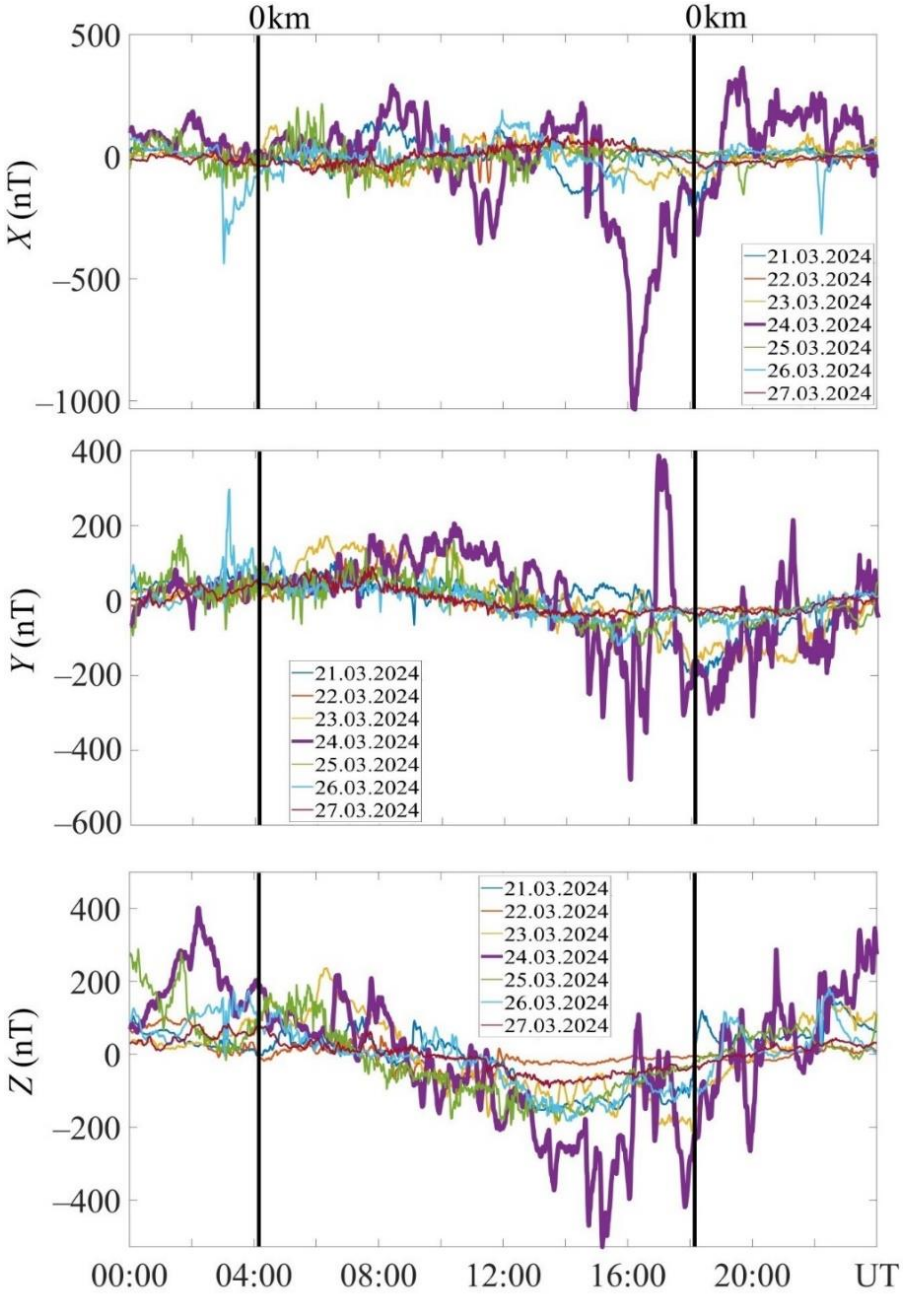

Figure A1. Temporal variations in the strength of the *X*, *Y*, and *Z* components of the geomagnetic field during March 21–27, 2024, at the HRN station (74.26° N geomagnetic) in the eastern hemisphere. The solid vertical lines indicate sunrise and sunset times at the ground.

https://doi.org/10.5194/egusphere-2025-4375
Preprint. Discussion started: 17 September 2025

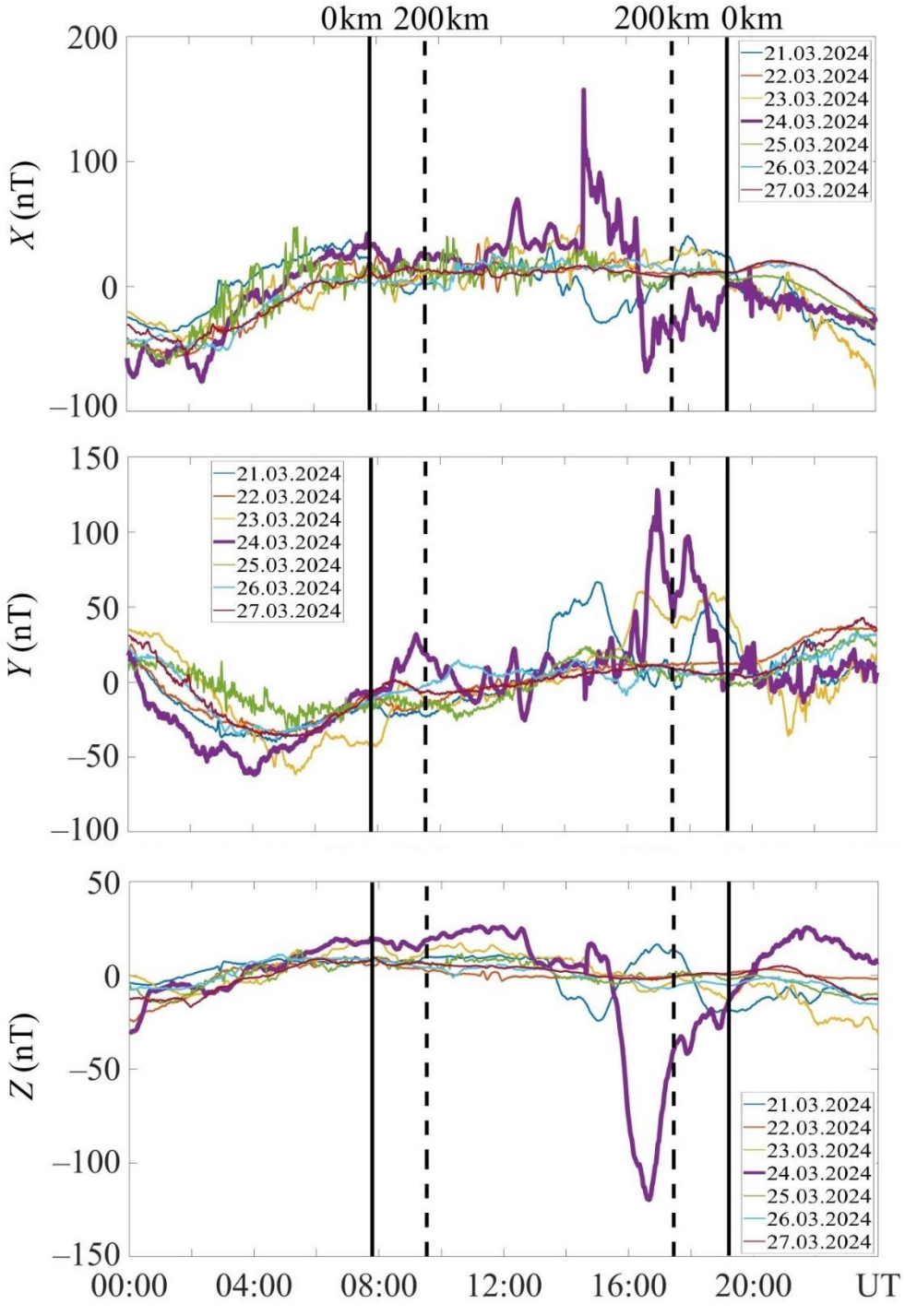

Figure A2. Temporal variations in the strength of the *X*, *Y*, and *Z* components of the geomagnetic field during March 21–27, 2024, at the PET station in the eastern hemisphere. The solid vertical lines indicate sunrise and sunset times at the ground, and the dashed vertical lines indicate those at 200 km altitude in the ionosphere.

https://doi.org/10.5194/egusphere-2025-4375
Preprint. Discussion started: 17 September 2025

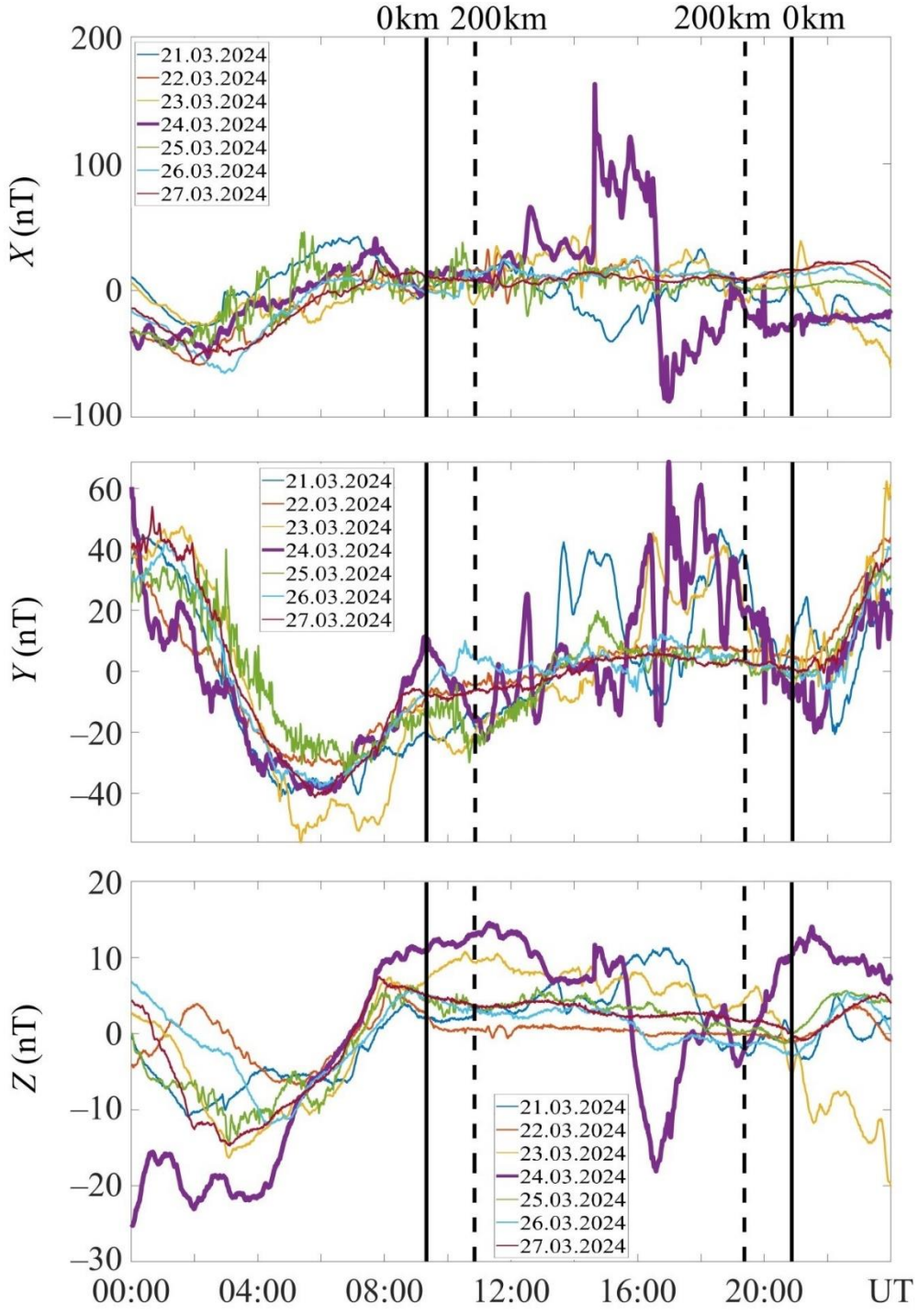

Figure A3. Temporal variations in the strength of the *X*, *Y*, and *Z* components of the geomagnetic field during March 21–27, 2024, at the KHB station in the eastern hemisphere. The solid vertical lines indicate sunrise and sunset times at the ground, and the dashed vertical lines indicate those at 200 km altitude in the ionosphere.

https://doi.org/10.5194/egusphere-2025-4375
Preprint. Discussion started: 17 September 2025

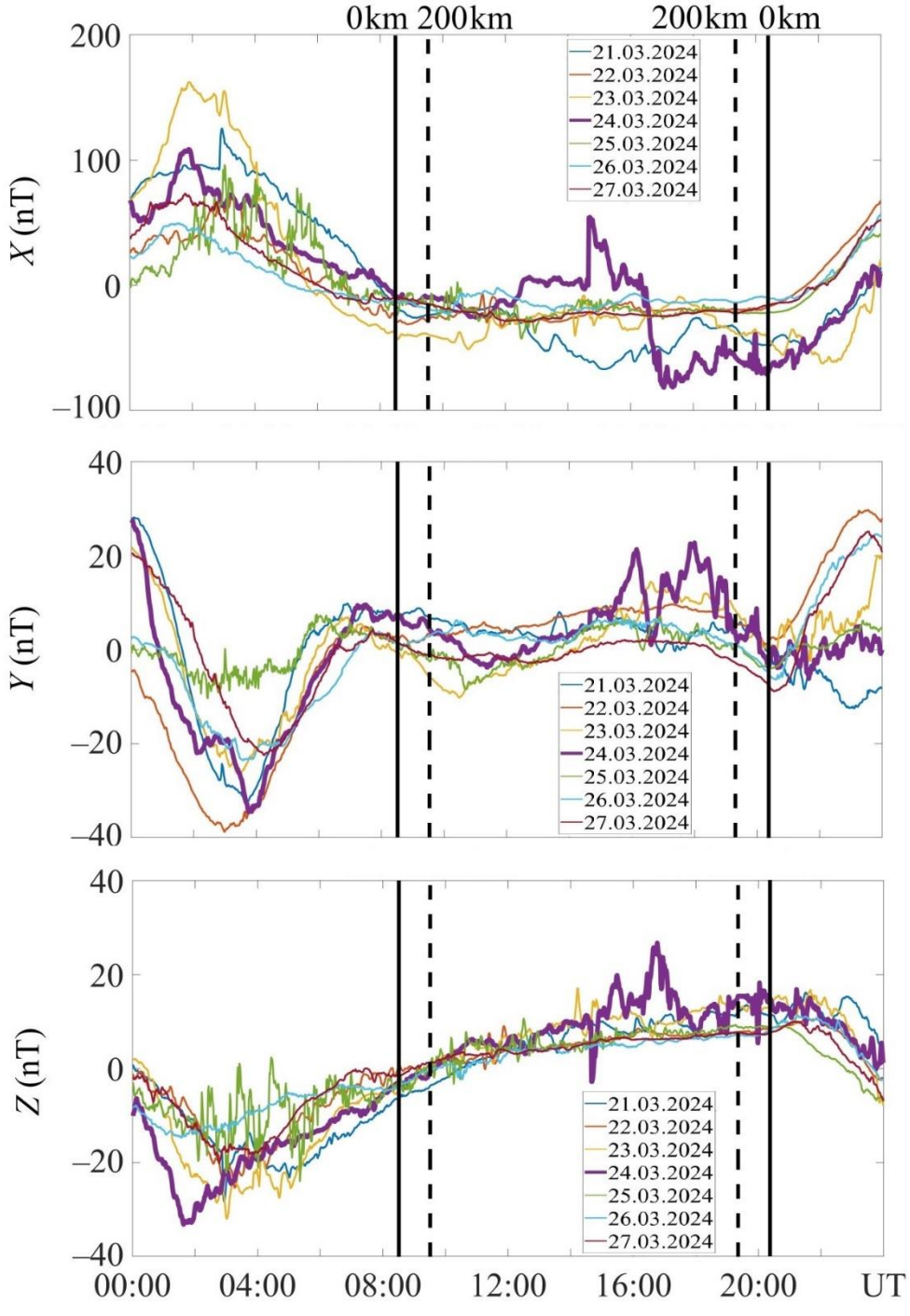

Figure A4. Temporal variations in the strength of the *X*, *Y*, and *Z* components of the geomagnetic field during March 21–27, 2024, at the GUA station in the eastern hemisphere. The solid vertical lines indicate sunrise and sunset times at the ground, and the dashed vertical lines indicate those at 200 km altitude in the ionosphere.

https://doi.org/10.5194/egusphere-2025-4375
Preprint. Discussion started: 17 September 2025

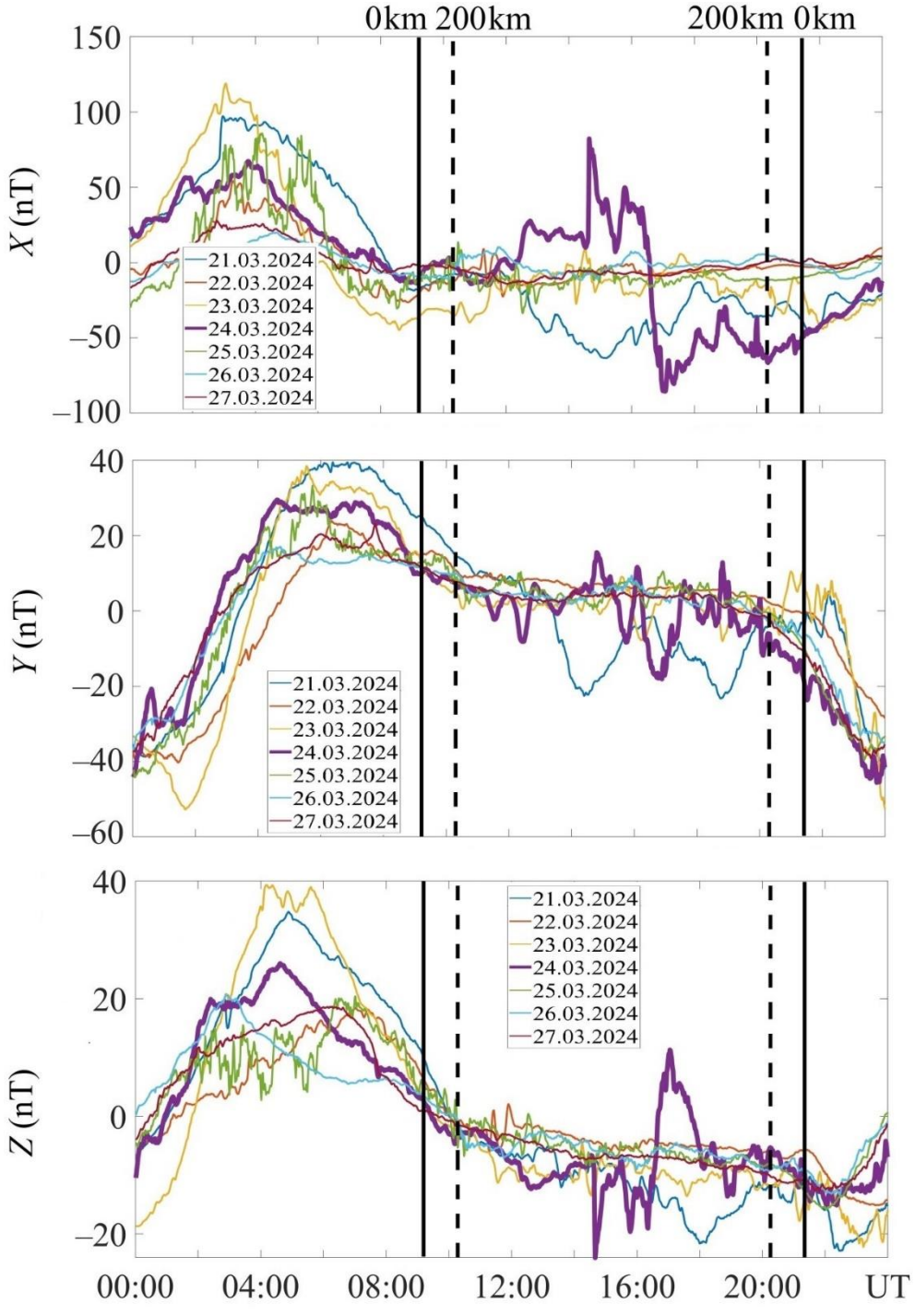

Figure A5. Temporal variations in the strength of the *X*, *Y*, and *Z* components of the geomagnetic field during March 21–27, 2024, at the KDU station in the eastern hemisphere. The solid vertical lines indicate sunrise and sunset times at the ground, and the dashed vertical lines indicate those at 200 km altitude in the ionosphere.

https://doi.org/10.5194/egusphere-2025-4375
Preprint. Discussion started: 17 September 2025

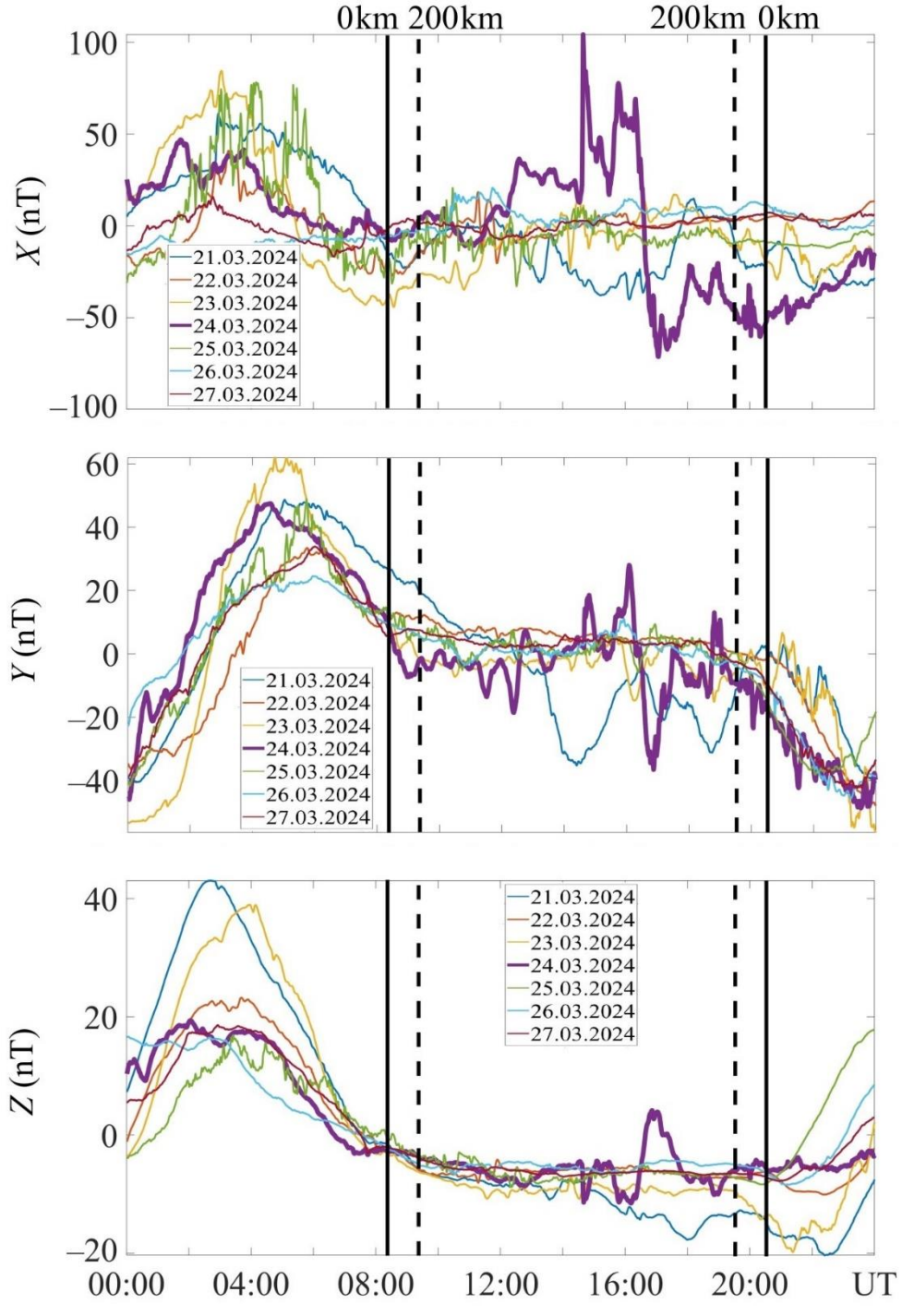

Figure A6. Temporal variations in the strength of the *X*, *Y*, and *Z* components of the geomagnetic field during March 21–27, 2024, at the CTA station in the eastern hemisphere. The solid vertical lines indicate sunrise and sunset times at the ground, and the dashed vertical lines indicate those at 200 km altitude in the ionosphere.

https://doi.org/10.5194/egusphere-2025-4375
Preprint. Discussion started: 17 September 2025

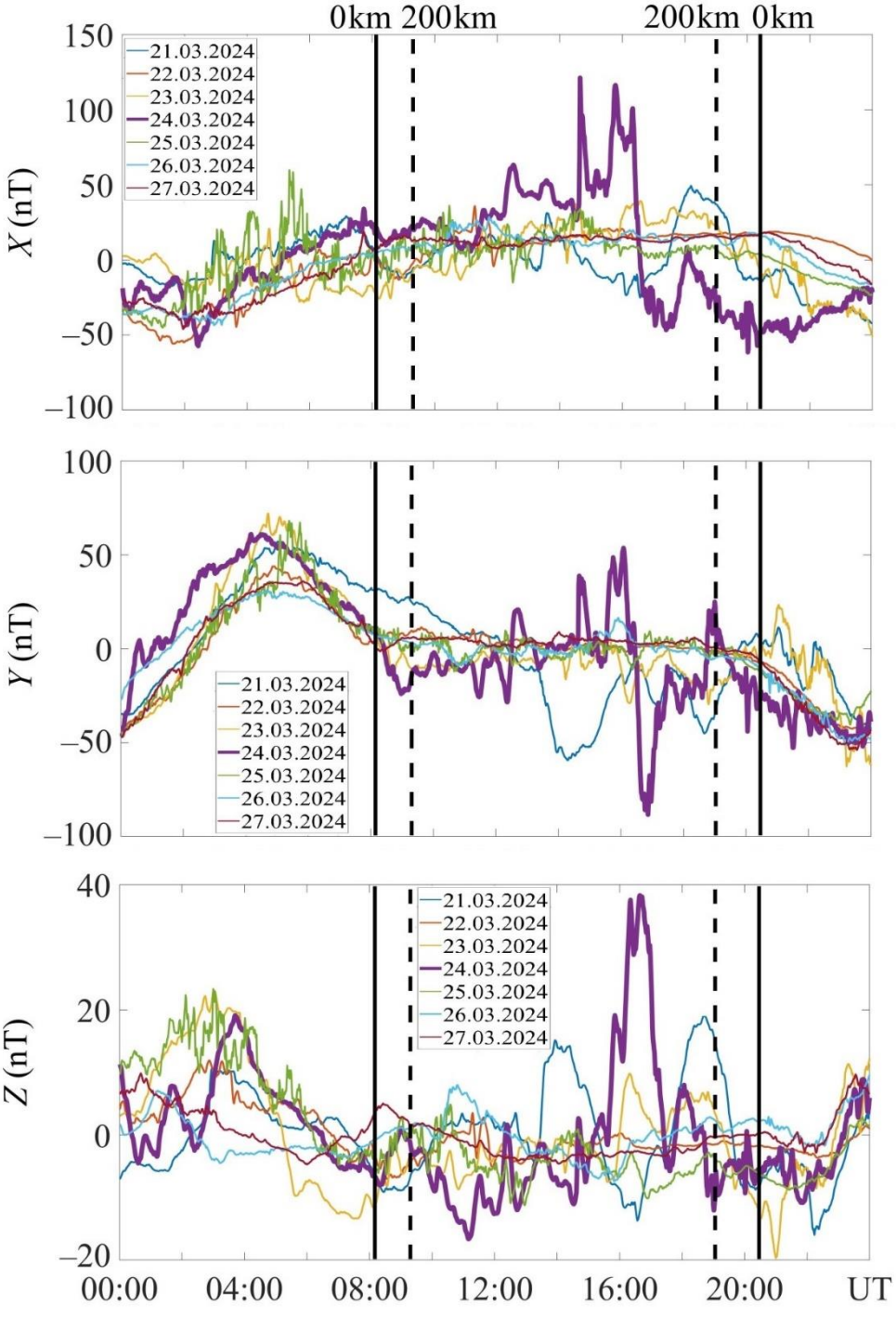

Figure A7. Temporal variations in the strength of the *X*, *Y*, and *Z* components of the geomagnetic field during March 21–27, 2024, at the CNB station in the eastern hemisphere. The solid vertical lines indicate sunrise and sunset times at the ground, and the dashed vertical lines indicate those at 200 km altitude in the ionosphere.

https://doi.org/10.5194/egusphere-2025-4375
Preprint. Discussion started: 17 September 2025

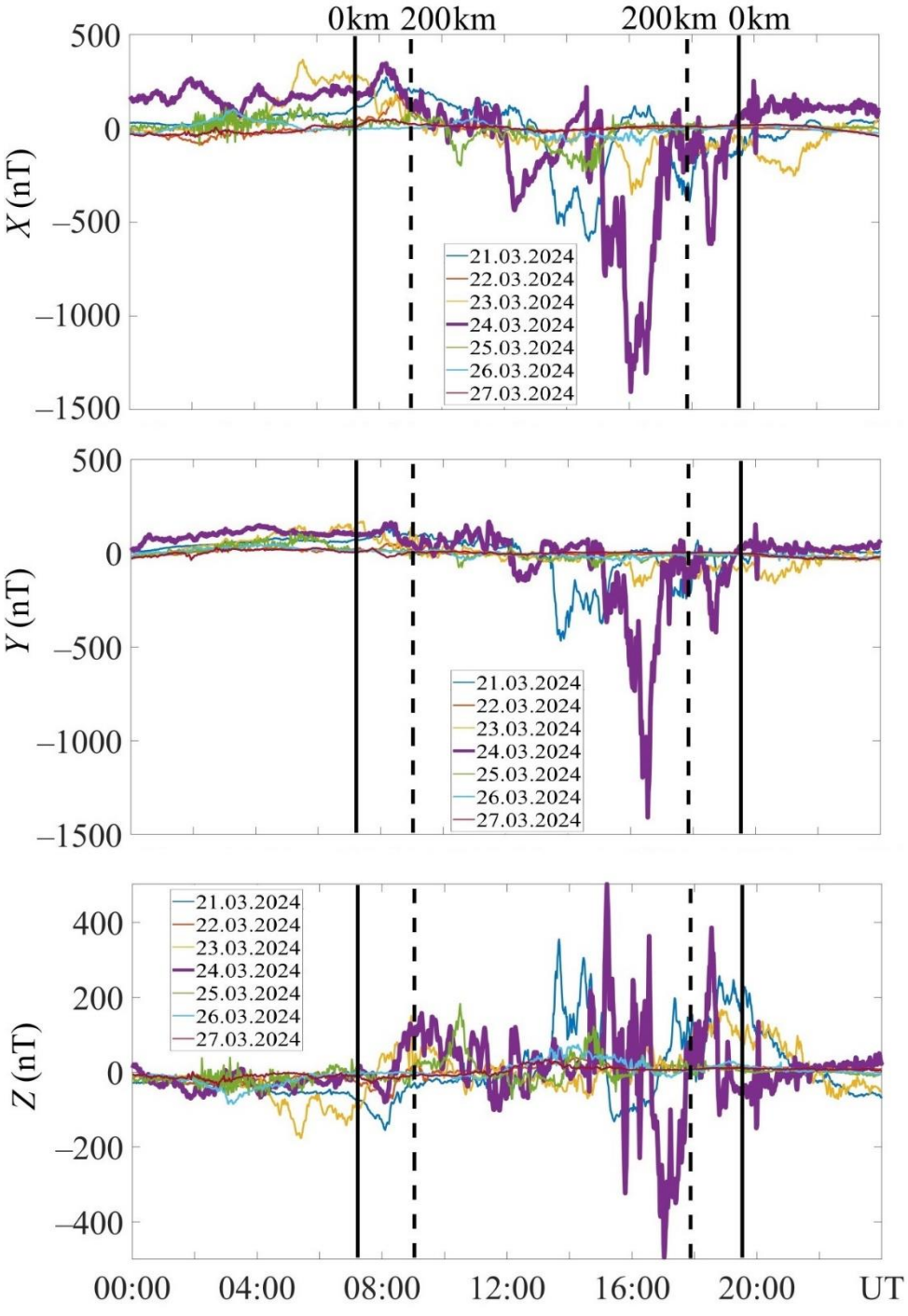

Figure A8. Temporal variations in the strength of the *X*, *Y*, and *Z* components of the geomagnetic field during March 21–27, 2024, at the MCQ station in the eastern hemisphere. The solid vertical lines indicate sunrise and sunset times at the ground, and the dashed vertical lines indicate those at 200 km altitude in the ionosphere.

https://doi.org/10.5194/egusphere-2025-4375
Preprint. Discussion started: 17 September 2025

Appendix B

Figures B1–B8 show temporal variations in the strength of the *X*, *Y*, and *Z* components of the geomagnetic field during March 21–27, 2024, in the western hemisphere.

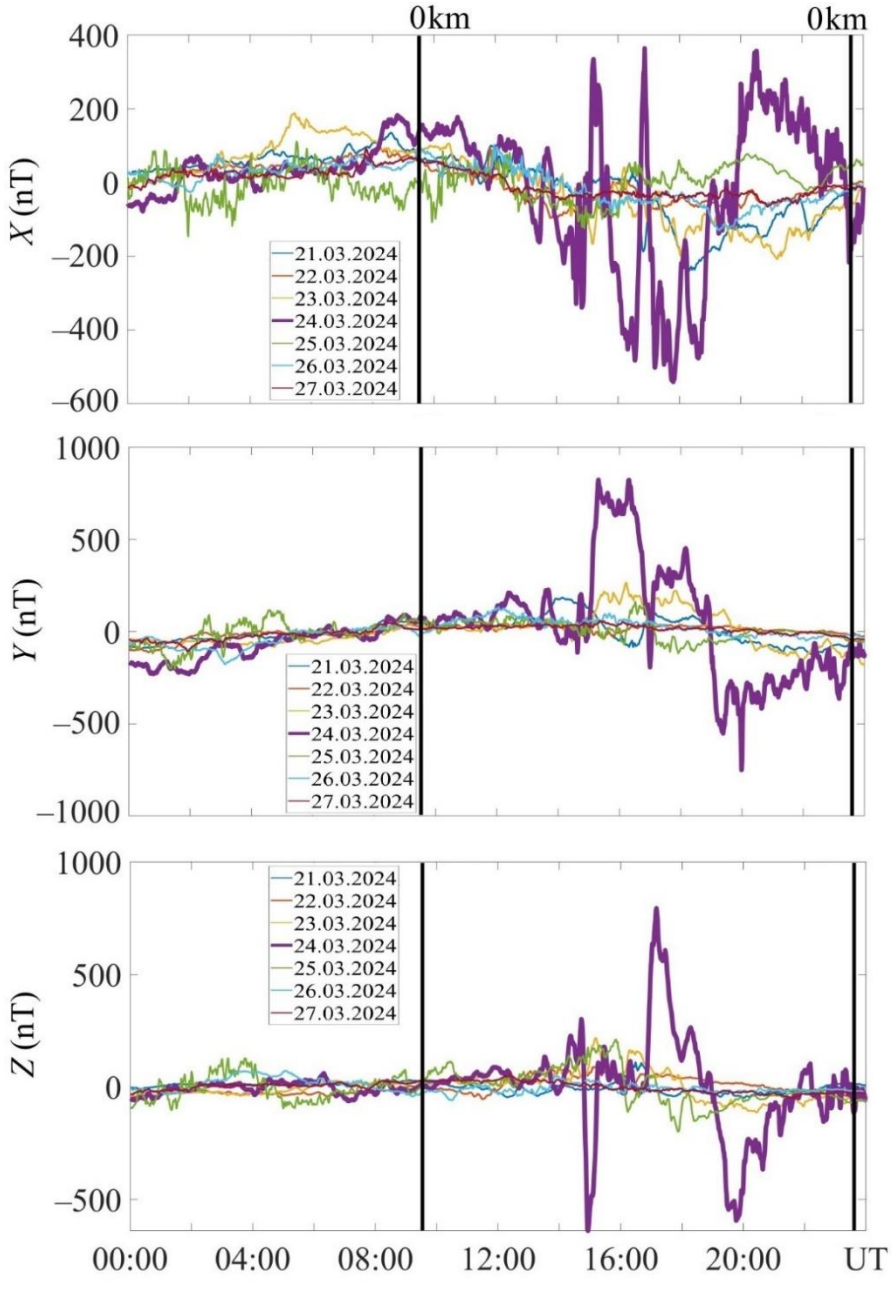

Figure B1. Temporal variations in the strength of the *X*, *Y*, and *Z* components of the geomagnetic field during March 21–27, 2024, at the THL station in the western hemisphere. The solid vertical lines indicate sunrise and sunset times at the ground.

https://doi.org/10.5194/egusphere-2025-4375
Preprint. Discussion started: 17 September 2025

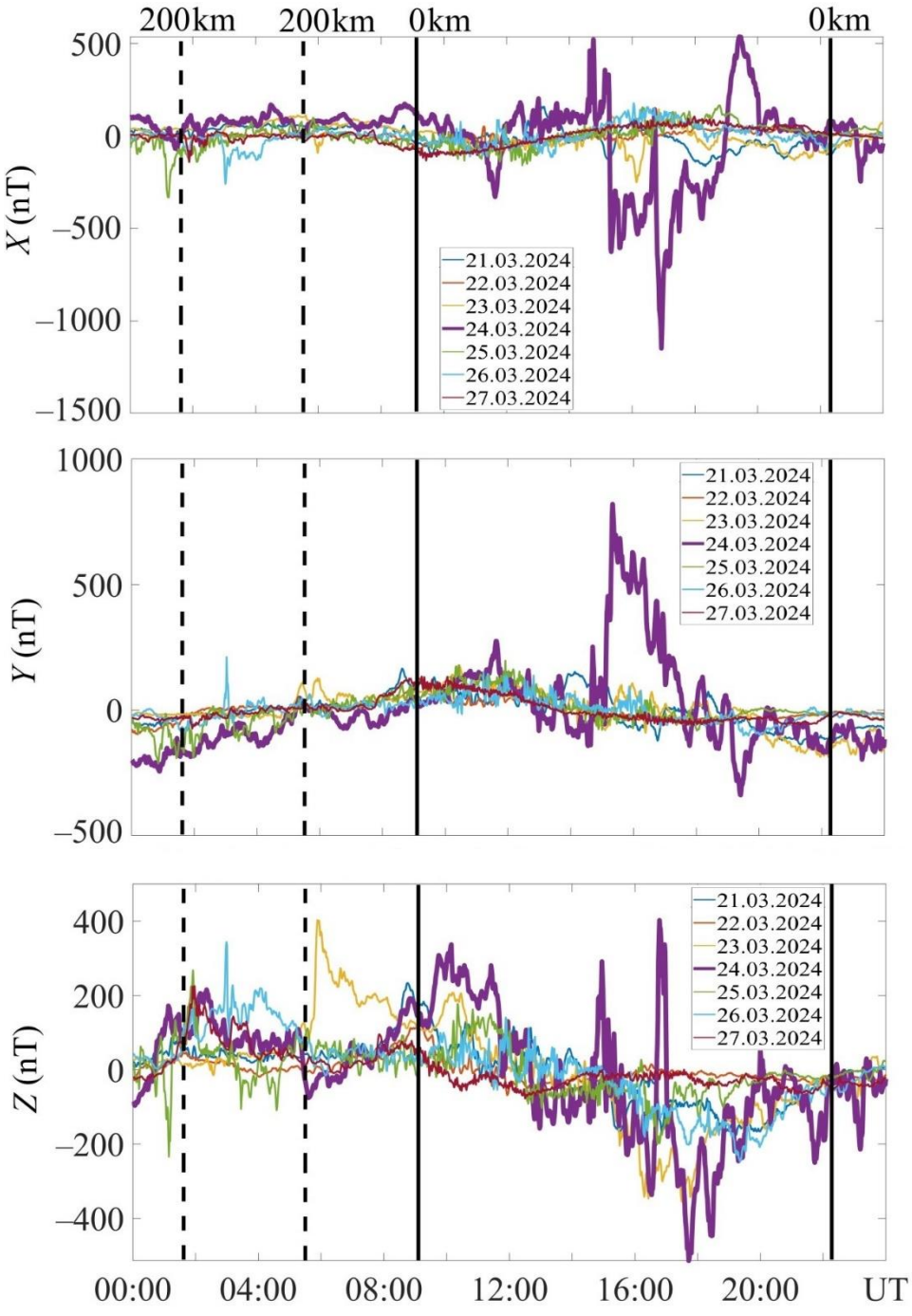

Figure B2. Temporal variations in the strength of the *X*, *Y*, and *Z* components of the geomagnetic field during March 21–27, 2024, at the GDH station in the western hemisphere. The solid vertical lines indicate sunrise and sunset times at the ground, and the dashed lines indicate those at 200 km altitude in the ionosphere.

https://doi.org/10.5194/egusphere-2025-4375
Preprint. Discussion started: 17 September 2025

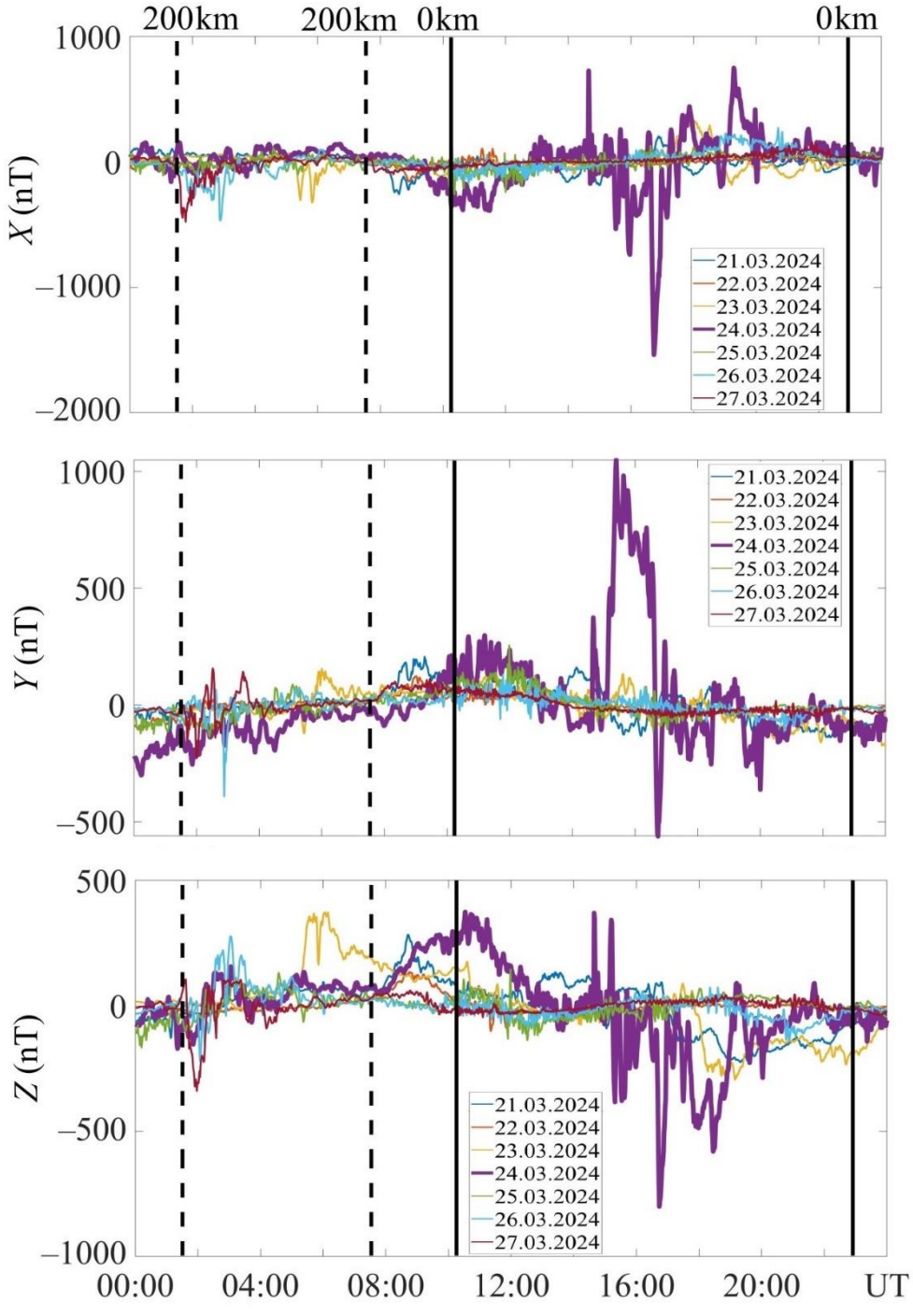

Figure B3. Temporal variations in the strength of the *X*, *Y*, and *Z* components of the geomagnetic field during March 21–27, 2024, at the IQA station in the western hemisphere. The solid vertical lines indicate sunrise and sunset times at the ground, and the dashed lines indicate those at 200 km altitude in the ionosphere.

https://doi.org/10.5194/egusphere-2025-4375
Preprint. Discussion started: 17 September 2025

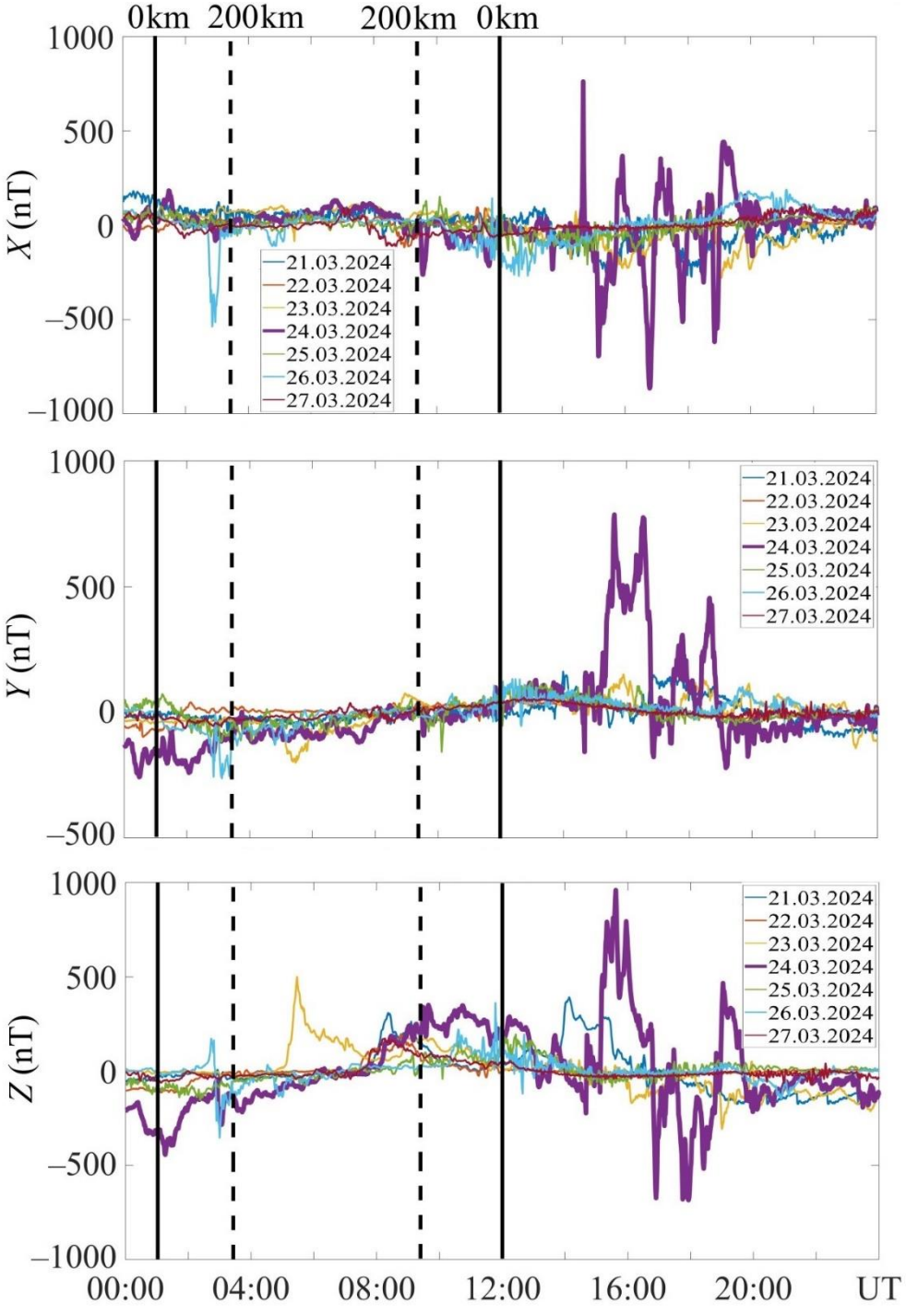

Figure B4. Temporal variations in the strength of the *X*, *Y*, and *Z* components of the geomagnetic field during March 21–27, 2024, at the BLC station in the western hemisphere. The solid vertical lines indicate sunrise and sunset times at the ground, and the dashed lines indicate those at 200 km altitude in the ionosphere.

https://doi.org/10.5194/egusphere-2025-4375
Preprint. Discussion started: 17 September 2025

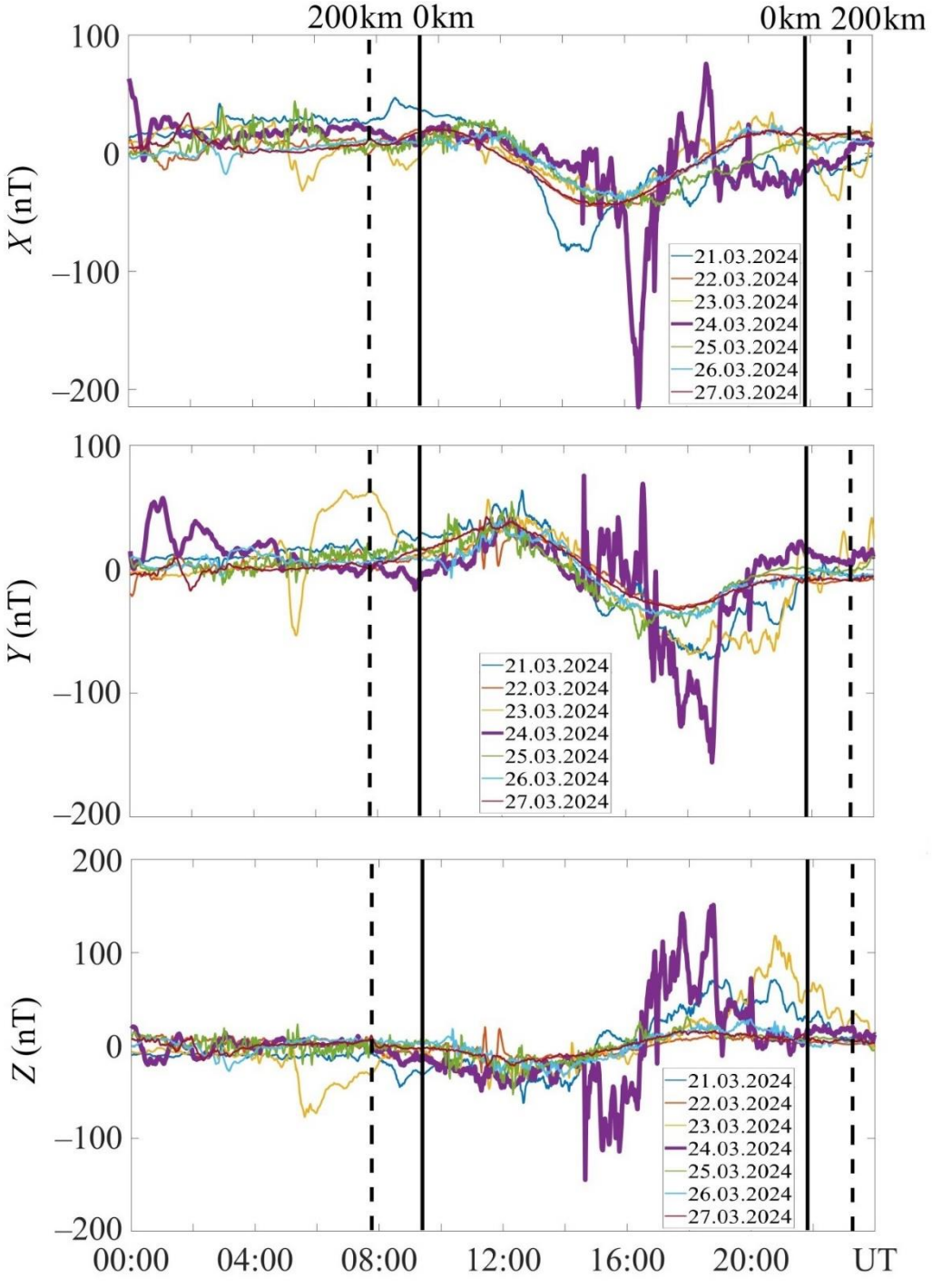

Figure B5. Temporal variations in the strength of the *X*, *Y*, and *Z* components of the geomagnetic field during March 21–27, 2024, at the STJ station in the western hemisphere. The solid vertical lines indicate sunrise and sunset times at the ground, and the dashed lines indicate those at 200 km altitude in the ionosphere.

https://doi.org/10.5194/egusphere-2025-4375
Preprint. Discussion started: 17 September 2025

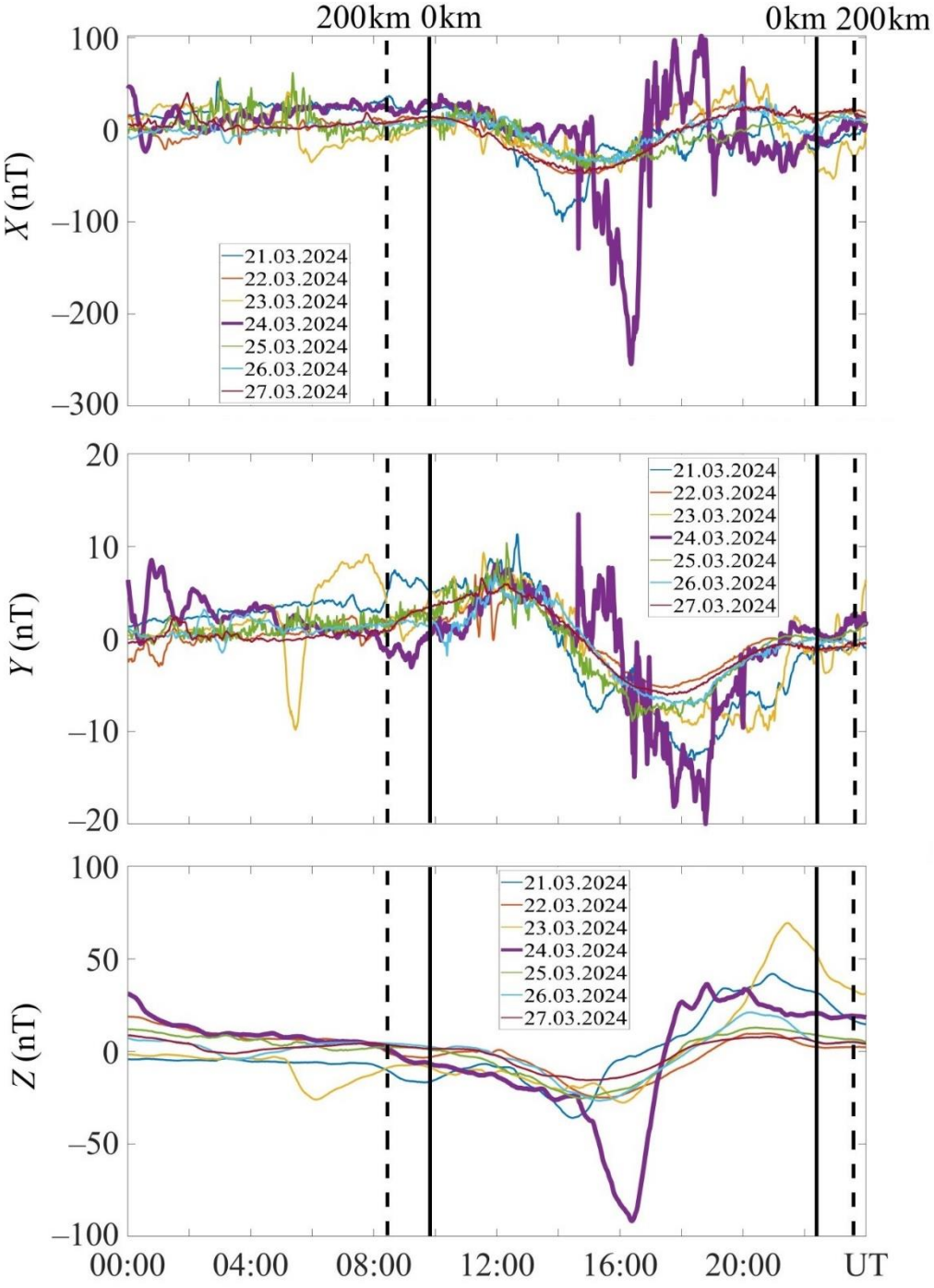

Figure B6. Temporal variations in the strength of the *X*, *Y*, and *Z* components of the geomagnetic field during March 21–27, 2024, at the SBL station in the western hemisphere. The solid vertical lines indicate sunrise and sunset times at the ground, and the dashed lines indicate those at 200 km altitude in the ionosphere.

https://doi.org/10.5194/egusphere-2025-4375
Preprint. Discussion started: 17 September 2025

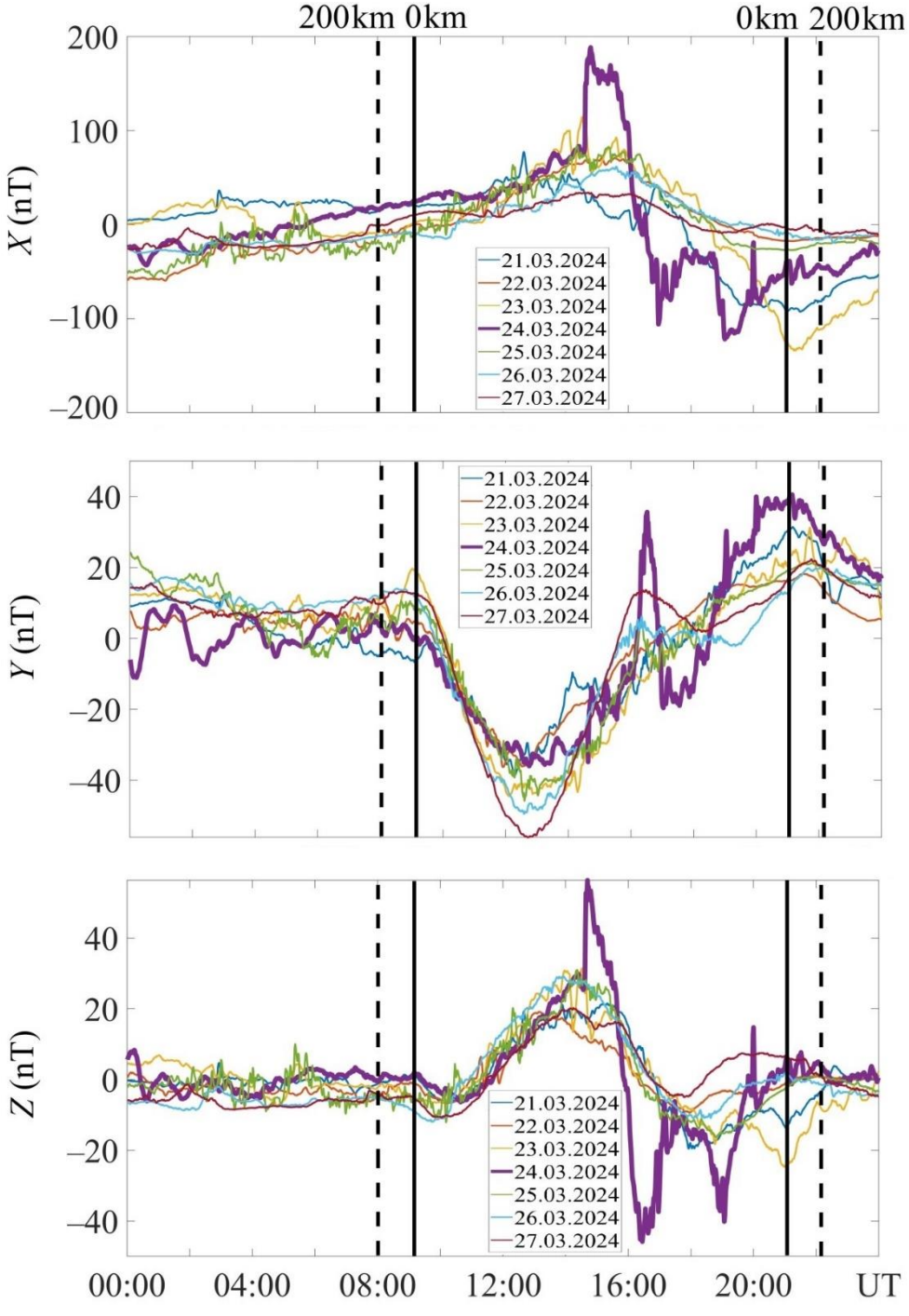

Figure B7. Temporal variations in the strength of the *X*, *Y*, and *Z* components of the geomagnetic field during March 21–27, 2024, at the VSS station in the western hemisphere. The solid vertical lines indicate sunrise and sunset times at the ground, and the dashed lines indicate those at 200 km altitude in the ionosphere.

https://doi.org/10.5194/egusphere-2025-4375
Preprint. Discussion started: 17 September 2025

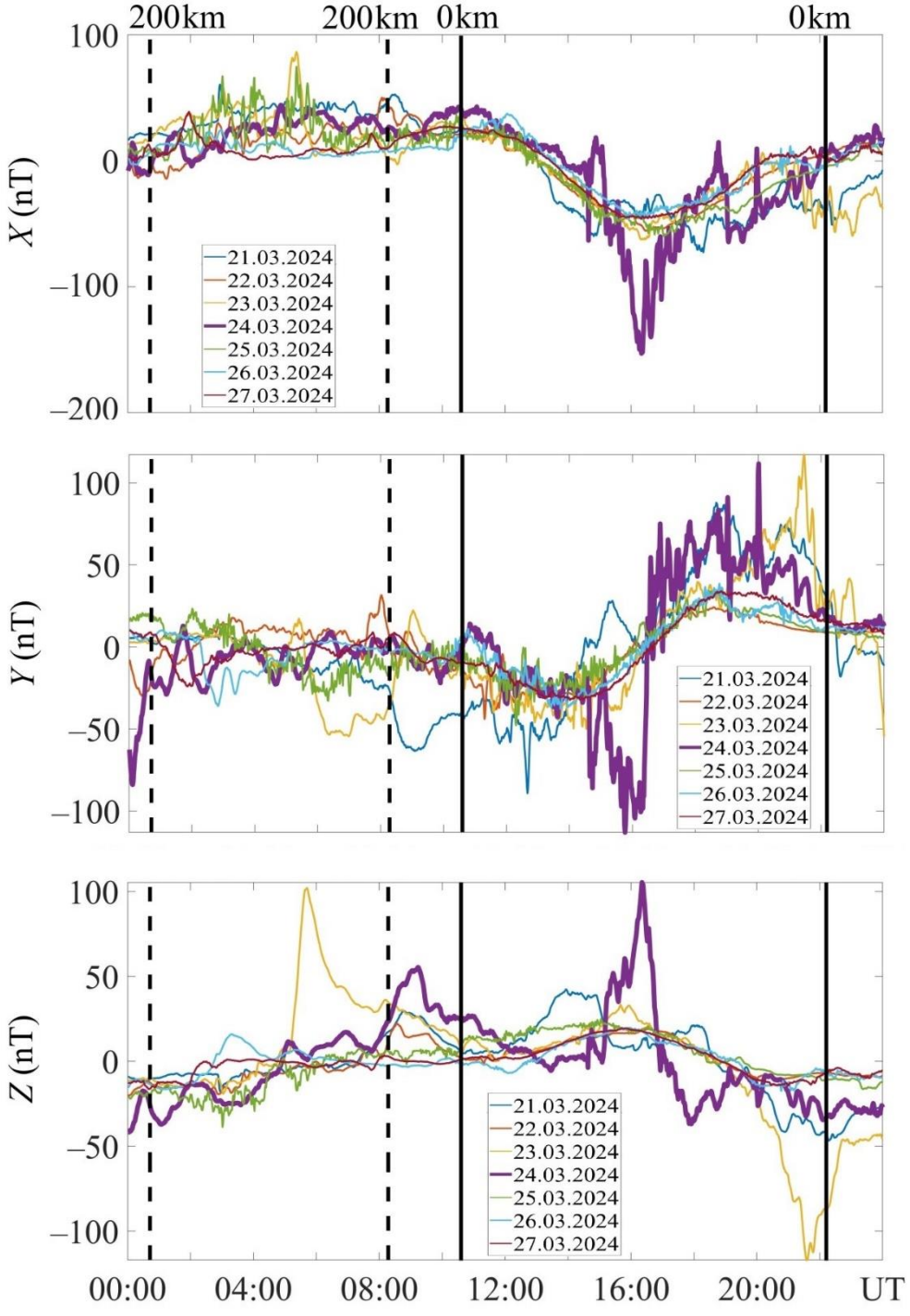

Figure B8. Temporal variations in the strength of the *X*, *Y*, and *Z* components of the geomagnetic field during March 21–27, 2024, at the AIA station in the western hemisphere. The solid vertical lines indicate sunrise and sunset times at the ground, and the dashed lines indicate those at 200 km altitude in the ionosphere.

https://doi.org/10.5194/egusphere-2025-4375
Preprint. Discussion started: 17 September 2025

Data availability. All data used in this study are publicly available. This publication makes use of data collected by INTERMAGNET and published at https://imag-data.bgs.ac.uk/GIN_V1/GINForms2. Information on the observatories is taken from https://intermagnet.org/metadata/#/imos. The solar wind parameters have been retrieved from the Goddard Space Flight Center Space Physics Data Facility https://omniweb.gsfc.nasa.gov/form/dx1.html.

Competing interests. The author declare that he has no conflict of interest.

Acknowledgments. The results presented in this paper rely on data collected at magnetic observatories. We thank the national institutes that support them and INTERMAGNET for promoting high standards of magnetic observatory practice. The author acknowledge the use of data and services provided by the NASA Goddard Space Flight Center Space Physics Data Facility (SPDF). The author is grateful to M. Yu. Holub, Y. H. Zhdanko and V. T. Rozumenko for assistance in preparing the manuscript.

Financial support. Work by L. F. Chernogor was supported by Ministry of Education and Science of Ukraine research project #0124U000478.

References

Aa, E., Zhang, S. R., Lei, J., et al.: Significant Midlatitude Plasma Density Peaks and Dual-Hemisphere SED During the 10–11 May 2024 Super Geomagnetic Storm, J. Geophys. Res. Space Phys., 129, 1–16, doi:10.1029/2024JA033360, 2024.

Adushkin, V. V., Spivak, A. A., Rybnov, Yu. S., et al.: Disturbance of Geophysical Fields and the Ionosphere during a Strong Geomagnetic Storm on April 23, 2023, Dokl. Earth Sci., 512, 1039–1043, doi:10.1134/S1028334X23601542, 2023.

Agyei-Yeboah, E., Fagundes, P. R., Tardelli, A. et al.: Global ionospheric response to a G2 and a G3 geomagnetic storms of November 4 and 5 2023, Advances in Space Research, 75, 5580–5602, doi:10.1016/j.asr.2025.01.046, 2025.

Akasofu, S.-I.: Electrodynamics of the magnetosphere: Geomagnetic storms, Space Sci. Rev., 6, 21–143, doi:10.1007/BF00213406, 1966.

Bojilova, R., Mukhtarov, P., and Pancheva, D.: Global Ionospheric Response During Extreme Geomagnetic Storm in May 2024, Remote Sens., 16, 4046, doi:10.3390/rs16214046, 2024.

Chernogor, L. F.: A two-step geospace storm as a new tool for experimentally estimating the threshold condition for the formation of a substorm current wedge, Ann. Geophys., 43, 15–35, doi:10.5194/angeo-43-15-2025, 2025a.

Chernogor, L. F.: Energetics of the Geospace Storm of April 23–24, 2023: from Solar Storm to Lithospheric Disturbance, Kinem. Phys. Celest. Bodies, 41, 3–19, doi:10.3103/S088459132503002X, 2025b.

Chernogor, L. F.: Energetics of Physical Processes Operated on May 8–12, 2024: From the Solar Storm to Lithospheric Disturbances, Adv. Space Res., 75, 4825–4849, doi:10.1016/j.asr.2024.12.069, 2025c.

Chernogor, L. F. and Bessarabova, V. O.: Global manifestations of a unique geospace storm on May 10–13, 2024 in the F-region of the ionosphere, Kinem. Phys. Celest. Bodies, 41, 209–220, doi:10.3103/S0884591325050022, 2025.

Chernogor, L. F. and Tkachenko, M. Yu.: Global variations of total electron content during the ionospheric storm on November 5, 2023, Astron. Space Phys. Kyiv Univ. Book Abstr., Int. Conf. Science Day Ukraine, May 28–31, 76–78, 2024.

Chernogor, L. F., Garmash, K. P., Guo, Q., et al.: Ionospheric effects of the 23–24 April 2023 geospace storm captured by the multifrequency multiple path software-defined radio system at oblique incidence over the People's Republic of China, J. Atmos. Sol.-Terr. Phys., 274, 106598, doi:10.1016/j.jastp.2025.106598, 2025a.

Chernogor, L. F., Rozumenko, V. T., Shevelev, M. B., et al.: Global geomagnetic response to the extreme geospace storm of May 10–11, 2024, Adv. Space Res., 76, 939–967, doi:10.1016/j.asr.2025.05.004, 2025b.

Correira, J., Evans, J. S., Lumpe, J. D., et al.: Upper atmospheric vortices following strong geomagnetic storms, Geophysical Research Letters, 52, e2024GL113726, doi:10.1029/2024GL113726, 2025.

Danilov, A. D.: Reaction of F region to geomagnetic disturbances (review) (in Russian). Heliogeophysical research, 5, 1–33, URL: http://vestnik.geospace.ru/index.php?id=189, 2013.

https://doi.org/10.5194/egusphere-2025-4375
Preprint. Discussion started: 17 September 2025

Despirak, I., Setsko, P., Lubchich, A., et al.: Geomagnetically induced currents (GICs) during strong geomagnetic activity (storms, substorms, and magnetic pulsations) on 23–24 April 2023, J. Atmos. Sol.-Terr. Phys., 261, 106293, doi:10.1016/j.jastp.2024.106293, 2024.
Evans, J. S., Correira, J., Lumpe, J. D., et al.: GOLD observations of the thermospheric response to the 10–12 May 2024 geomagnetic storm, ESS Open Archive, Geophys. Res. Lett., 51, 1–9, doi:10.22541/essoar.171926407.71074494/v1, 2024.
Ghag, K., Raghav, A., Bhaskar, A., et al.: Quasi-planar ICME sheath: A cause of first two-step extreme geomagnetic storm of 25th solar cycle observed on 23 April 2023, Adv. Space Res., 73, 6288–6297, doi:10.1016/j.asr.2024.03.011, 2024.
Gonzalez, W. D., Jozelyn, J. A., Kamide, Y., et al.: What is a geomagnetic storm?, J. Geophys. Res., 99, 5771–5792, doi:10.1029/93JA02867, 1994.
Grandin, M., Bruus, E., Ledvina, V. E., et al.: The geomagnetic superstorm of 10 May 2024: Citizen science observations, EGUsphere [preprint], doi:10.5194/egusphere-2024-2174, 2024.
Guo, X., Zhao, B. Q., Yu, T. T., et al.: East–West difference in the ionospheric response during the recovery phase of May 2024 super geomagnetic storm over the East Asian, J. Geophys. Res.: Space Phys., 129, e2024JA033170, doi:10.1029/2024JA033170, 2024.
Hajra, R., Tsurutani, B. T., Lu, Q., et al.: The April 2023 SYM-H = −233 nT Geomagnetic storm: A classical event, Journal of Geophysical Research: Space Physics, 129, e2024JA032986, doi:10.1029/2024JA032986, 2024a.
Hajra, R., Tsurutani, B. T., Lakhina, G. S., et al.: Interplanetary Causes and Impacts of the 2024 May Superstorm on the Geosphere: An Overview, Astrophys. J., 974, 1–12, doi:10.3847/1538-4357/ad7462, 2024b.
Hayakawa, H., Ebihara, Y., Mishev, A., et al.: The Solar and Geomagnetic Storms in May 2024: A Flash Data Report, arXiv [astro-ph.SR], doi:10.48550/arXiv.2407.07665, 2024.
Hu, P., Chen, G., Zhang, S., et al.: Low-latitude ionospheric responses to the severe geomagnetic storm during 23–25 april 2023 over the American sector, Journal of Geophysical Research: Space Physics, 130, e2024JA033692, doi:10.1029/2024JA033692, 2025.
Huang, F., Lei, J., Yue, X., et al.: Interplay of Gravity Waves and Disturbance Electric Fields to the Abnormal Ionospheric Variations During the 11 May 2024 Superstorm, AGU Adv., 6, 1–15, doi:10.1029/2024AV001379, 2025.
INTERMAGNET Technical Reference Manual, Version 5.0.0, St-Louis, B. (Ed.), INTERMAGNET Operations Committee and Executive Council, URL: https://gfzpublic.gfz-potsdam.de/rest/items/item_5008881_7/component/file_5008886/content, 2020.
Karan, D. K., Martinis, C. R., Daniell, R. E., et al.: GOLD Observations of the Merging of the Southern Crest of the Equatorial Ionization Anomaly and Aurora During the 10–11 May 2024 Mother's Day Super Geomagnetic Storm, ESS Open Archive, doi:10.22541/essoar.171805504.42893378/v1, 2024.
Kilpua, E., Koskinen, H. E. J., and Pulkkinen, T. I.: Coronal mass ejections and their sheath regions in interplanetary space, Living Rev. Sol. Phys., 14, 5, doi:10.1007/s41116-017-0009-6, 2017.
Kim, J.-H., Kwak, Y.-S., Kim, Y., and Jee, G.: Analysis of the Energy Inflow into High-Latitude Regions during the Geomagnetic Storm Period on November 3–4, 2021, AGU Fall Meeting 2023, San Francisco, USA, Dec. 11–15, id. SA31B-2849, URL: https://agu.confex.com/agu/fm23/meetingapp.cgi/Paper/1405852, 2023a.
Kim, J., Kwak, Y. S., Lee, C., et al.: Observational evidence of thermospheric wind and composition changes and the resulting ionospheric disturbances in the European sector during extreme geomagnetic storms, J. Space Weather Space Clim., 13, 24, doi:10.1051/swsc/2023025, 2023b.
King, J. H. and Papitashvili, N. E.: Solar wind spatial scales in and comparisons of hourly Wind and ACE plasma and magnetic field data, J. Geophys. Res., 110, A02209, doi:10.1029/2004JA010649, 2005.
Kruparova, O., Krupar, V., Szabo, A., et al.: Unveiling the Interplanetary Solar Radio Bursts of the 2024 Mother's Day Solar Storm, Astrophys. J. Lett., 970, L13, 1–7, doi:10.3847/2041-8213/ad5da6, 2024.
Laštovička, J.: Effects of geomagnetic storms – different morphology and origin in the upper middle atmosphere and the troposphere, Studia Geophysica et Geodaetica, 41, 73–81, doi:10.1023/A:1023340824496, 1997.
Lugaz, N., Farrugia, C. J., Smith, C. W., and Paulson, K.: Shocks inside CMEs: a survey of properties from 1997 to 2006, J. Geophys. Res., 120, 2409–2427, doi:10.1002/2014JA020848, 2015.
Lugaz, N., Temmer, M., Wang, Y., and Farrugia, C. J.: The interaction of successive coronal mass ejections: a review, Sol. Phys., 292, 64, doi:10.1007/s11207-017-1091-6, 2017.
Manchester, W. B. IV, Kilpua, E. K. J., Liu, Y. D., et al.: The physical processes of CME/ICME evolution, Space Sci. Rev., doi:10.1007/s11214-017-0394-0, 2017.
Mavromichalaki, H., Papailiou, M.-C., and Livada, M.: Unusual Forbush Decreases and Geomagnetic Storms on 24 March, 2024 and 11 May, 2024, Atmosphere, 15, 1033, doi:10.3390/atmos15091033, 2024.
Mendillo, M.: Storms in the ionosphere: Patterns and processes for total electron content, Rev. Geophys., 44, RG4001, doi:10.1029/2005RG000193, 2006.
Mlynczak, M. G., Hunt, L. A., Nowak, N., et al.: Global thermospheric infrared response to the Mother's day weekend extreme storm of 2024, Geophysical Research Letters, 51, e2024GL110701, doi:10.1029/2024GL110701, 2024.
Myllys, M., Kilpua, E. K. J., Lavraud, B., and Pulkkinen, T. I.: Solar wind-magnetosphere coupling efficiency during ejecta and sheath-driven geomagnetic storms, J. Geophys. Res., 121, 4378–4396, doi:10.1002/2016JA022407, 2016.

https://doi.org/10.5194/egusphere-2025-4375
Preprint. Discussion started: 17 September 2025

Palmerio, E., Kilpua, E. K. J., Savani, N. P.: Planar magnetic structures in coronal mass ejection-driven sheath regions, Ann. Geophys., 34, 313–322, doi:10.5194/angeo-34-313-2016, 2016.
Parker, W. E., Linares, R., et al.: Satellite Drag Analysis During the May 2024 Gannon Geomagnetic Storm, arXiv [astro-ph.EP], doi:10.48550/arXiv.2406.08617, 2024.
Pierrard, V., Verhulst, T. G. W., and Chevalier, J.-M.: Effects of the Geomagnetic Superstorms of 10–11 May 2024 and 7–11 October 2024 on the Ionosphere and Plasmasphere, Atmosphere, 16, 299, doi:10.3390/atmos16030299, 2025.
Ponomarchuk, S. N. and Zolotukhina, N. A.: Disturbances of ionospheric radio channel during geomagnetic storms in November–December 2023, Sol.-Terr. Phys., 10, 84–98, doi:10.12737/stp-104202410, 2024.
Ram, S. T., Veenadhari, B., Dimri, A. P., et al.: Super-Intense Geomagnetic Storm on 10–11 May 2024: Possible Mechanisms and Impacts, Space Weather, 22, 1–14, doi:10.1029/2024SW004126, 2024.
Ranjan, A. K., Nailwal, D., Sunil Krishna, M. V., et al.: Evidence of potential thermospheric overcooling during the May 2024 geomagnetic superstorm, Journal of Geophysical Research: Space Physics, 129, e2024JA033148, doi:10.1029/2024JA033148, 2024.
Regi, M., Perrone, L., Del Corpo, A., et al.: Space Weather Effects Observed in the Northern Hemisphere during November 2021 Geomagnetic Storm: The Impacts on Plasmasphere, Ionosphere and Thermosphere Systems, Remote Sens., 14, 5765, doi:10.3390/rs14225765, 2022.
Singh, R., Scipion, D. E., Kuyeng, K., et al.: Ionospheric Disturbances observed over the Peruvian sector during the Mother's Day Storm (G5-level) on May 10–12, 2024, ESS Open Archive, doi:10.22541/essoar.172108210.04033367/v1, 2024.
Souza, J. R., Dandenault, P., Santos, A. M., et al.: Impacts of Storm Electric Fields and Traveling Atmospheric Disturbances Over the Americas During 23–24 April 2023 Geomagnetic Storm: Experimental Analysis, J. Geophys. Res. Space Phys., 129, 1–16, doi:10.1029/2024JA032698, 2024.
Spogli, L., Alberti, T., Bagiacchi, P., et al.: The effects of the May 2024 Mother's Day superstorm over the Mediterranean sector: from data to public communication, Annals of Geophysics, 67, PA218, doi:10.4401/ag-9117, 2024.
Sun, W., Li, G., Zhang, S.-R., et al.: Complex ionospheric fluctuations over East and Southeast Asia during the May 2024 super geomagnetic storm, Journal of Geophysical Research: Space Physics, 129, e2024JA033096, doi:10.1029/2024JA033096, 2024.
Terefe, D. A., Gereme, M. N., and Habarulema, J. B.: Latitudinal variation of ionospheric storm effects on March 22–24, 2024 geomagnetic storm over the African Sector, Advances in Space Research, 76, 2913–2925, doi:10.1016/j.asr.2025.06.047, 2025.
Themens, D. R., Elvidge, S., McCaffrey, A., et al.: The high latitude ionospheric response to the major May 2024 geomagnetic storm: A synoptic view, Geophysical Research Letters, 51, e2024GL111677, doi:10.1029/2024GL111677, 2024.
Tilahun, A. M., Uluma, E., and Ejigu, Y. G.: Variation of Total Electron Content During a Severe Geomagnetic Storm of 23–24 April 2023, Res. Square, 1–20, doi:10.21203/rs.3.rs-5332574/v1, 2023.
Vichare, G. and Bagiya, M. S.: Manifestations of strong IMF-By on the equatorial ionospheric electrodynamics during 10 May 2024 geomagnetic storm, Geophys. Res. Lett., 51, 1–6, doi:10.1029/2024GL112569, 2024.
Wu, F., Yao, Di, and Yu, C.: An investigation into the influence of solar flares and geomagnetic storms on the F2 layer of the ionosphere in Western Europe during March 2024, Advances in Space Research, 75, 936–952, doi:10.1016/j.asr.2024.09.027, 2025.
Xia, H., Wang, H., and Zhang, K.: Extreme Responses of the Ionospheric Radial Currents to the Main Phase of the Super Geomagnetic Storm on 10 May 2024, J. Geophys. Res. Space Phys., 129, e2024JA033126, 1–12, doi:10.1029/2024JA033126, 2024.
Yamazaki, Y., Matzka, J., Da Silva, M. V. S., et al.: Assessment of Geomagnetic Activity for the Kp=9 "Gannon Storm" in May 2024 Based on Version 3.0 Hpo Indices, ESS Open Archive, doi:10.22541/essoar.171838396.68563140/v1, 2024.
Yadav, V. K., Srikar, P. T., Vichare, G., et al.: The extreme solar transient events as observed by the MAG payload onboard Aditya-L1 Spacecraft around L1 Point, 1–30, doi:10.13140/RG.2.2.11518.29766, 2025.
Yan, Q. and Yao, H. B.: Recent geomagnetic storms observed by Macau Science Satellite-1, Earth Planet. Phys., 8, 565–569, doi:10.26464/epp2024047, 2024.
Zalizovski, A., Yampolski, Y., Stanislawska, I., et al.: Long-distance HF radio waves propagation during the April 2023 geomagnetic storm by measurements in Antarctica, in Europe, and aboard RV Noosfera, Ukrainian Antarctic Journal, 21, 190–209, doi:10.33275/1727-7485.2.2023.717, 2023.
Zhai, C., Tang, S., Peng, W., et al.: Driver of the Positive Ionospheric Storm over the South American Sector during 4 November 2021 Geomagnetic Storm, Remote Sensing, 15, 111, doi:10.3390/rs15010111, 2023.